

Paving the Way Towards Mobile IAB: Problems, Solutions and Challenges

Victor F. Monteiro, Fco. Rafael M. Lima, *Senior Member, IEEE*, Darlan C. Moreira, Diego A. Sousa, Tarcisio F. Maciel, Behrooz Makki, *Senior Member, IEEE*, and Hans Hannu

Abstract—Deploying access and backhaul as wireless links, a.k.a. integrated access and backhaul (IAB), is envisioned as a viable approach to enable flexible and dense networks. Even further, mobile IAB (mIAB) is a candidate solution to enhance the connectivity of user equipments (UEs) moving together. In this context, different of other works from the literature, the present work overviews the basis for the deployment of mIAB by presenting: 1) the current status of IAB standardization in the fifth generation (5G) new radio (NR); 2) a new taxonomy for state-of-the-art works regarding fixed IAB and mIAB; 3) an extensive performance analysis of mIAB based on simulation results; and 4) open challenges and potential future prospects of mIAB. Specifically, the proposed taxonomy classifies IAB works according to different perspectives and categorizes mIAB works according to the type of mobility. For each type of mobility, the main studied topics are presented. Regarding the performance evaluation, we consider an urban macro scenario where mIAB nodes are deployed in buses in order to improve the passengers connection. The results show that, compared to other network architectures, the deployment of mIAB nodes remarkably improves the passengers throughput and latency in both downlink and uplink.

Index Terms—5G standardization, 6G, backhaul, integrated access and backhaul (IAB), mobile IAB, mobility, moving cell.

I. INTRODUCTION

Fifth generation (5G) networks are being designed and deployed considering a dense deployment of small cells in order to simultaneously serve more user equipments (UEs) with higher throughput and lower delay [1]. However, building from scratch a completely new infrastructure is costly and takes time [2]. Deploying a wireless backhaul is then envisioned to be a technically viable approach to enable flexible and dense network deployments [3].

Wireless backhaul has already been considered in the past. However, on the one hand, it has been based on non-standardized solutions, deployed on millimeter wave (mmWave) apart of the spectrum used for access links and mainly designed for point-to-point (PTP) communications with good networking planning and line of sight (LOS) connections, as in [4]–[7]. On the other hand, in 5G, access links and backhaul may be deployed both in mmWave and

5G networks are expected to be dense, possibly unplanned and with low height access points, which requests the support of non-line of sight (NLOS) backhaul. These 5G characteristics are the main reasons why academia and industry are now investigating a standardized solution for joint access and backhaul fitting the 5G characteristics. The 3rd generation partnership project (3GPP), the organization in charge of standardizing 5G new radio (NR), has already started standardizing this new wireless backhaul under the term integrated access and backhaul (IAB).

IAB is promising and desirable due to its cost effectiveness¹, fast deployment and easy maintenance [8]. Regarding the cost, the authors of [9] compared the deployment cost of three typical backhaul technologies, i.e., wireless, direct fiber and passive optical. They showed that a wireless backhaul is the most cost-effective among the three backhaul technologies. Another advantage is the support of larger bandwidth in NR without the need to proportionally densify the supporting wired transport network [3].

Thinking further, IAB also allows the deployment of mobile cells, called here mobile IAB (mIAB), which should be available after 3GPP Release 18. The mIAB is expected to enhance the service of moving UEs improving connectivity to the network and to avoid signaling storms from simultaneous handover (HO) messages. Examples of mIAB applications are illustrated in Fig. 1, e.g., mIAB nodes deployed at trains, buses and unmanned aerial vehicles (UAVs)². In the examples presented in Fig. 1, the mIAB nodes are wirelessly served either by a base station (BS) which is connected by wire/fiber to the core network (CN) or even by a BS which is also wirelessly served by another wired-connected BS to the CN.

In terms of mobility, one can consider three distinct types of IAB nodes: fixed IAB nodes, nomadic IAB nodes and mIAB nodes. While fixed IAB nodes are always at the same position, allowing a system planning of long duration, nomadic IAB nodes adapt their location before the communication, remaining fixed during the communication. The main objective of nomadic IAB is to temporarily extend the coverage and serve out-vehicle UEs in a given area, e.g., disaster area, close to stadiums, etc. With mIAB, on the other hand, the mIAB node on top of, e.g., trains, buses, trams, may communicate during the movement. As opposed to nomadic IAB, the main goal for mIAB is to serve the in-vehicle UEs. In this work, we concentrate on mIAB.

This work was supported by Ericsson Research, Sweden, and Ericsson Innovation Center, Brazil, under UFC.49 Technical Cooperation Contract Ericsson/UFC. The work of Francisco R. M. Lima was supported by FUNCAP (edital BPI) under Grant BP4-0172-00245.01.00/20. The work of Tarcisio F. Maciel was supported by CNPq under Grant 312471/2021-1.

Victor F. Monteiro, Fco. Rafael M. Lima, Darlan C. Moreira, Diego A. Sousa and Tarcisio F. Maciel are with the Wireless Telecommunications Research Group (GTEL), Federal University of Ceará (UFC), Fortaleza, Ceará, Brazil. Diego A. Sousa is also with Federal Institute of Education, Science, and Technology of Ceará (IFCE), Paracuru, Brazil. Behrooz Makki and Hans Hannu are with Ericsson Research, Sweden.

¹The cost discussions and the details of the simulation parameter settings are not necessarily aligned with the Ericsson's points of interest.

²UAV-based communication will not be part of the Release 18 discussions on mIAB.

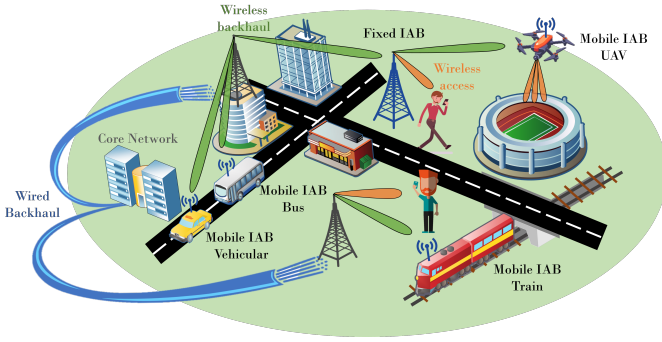


Fig. 1. Overview scenario presenting examples of fixed IAB and mIAB use cases.

In this context, the present work aims at presenting an overview on the topic of mIAB and on the technologies enabling its deployment at 5G networks and beyond. At the time of writing of this work, as far as we know, [10] is the unique survey focused on IAB, while [11] is the most complete survey covering mobile cells.

The work in [10] focuses on fixed IAB. As opposed, we concentrate on the potentials and challenges of mIAB. Particularly, 1) we review and propose a taxonomy for works on mIAB which was not covered by [10]. Also, 2) different from [10], we present deep performance evaluations to verify the potential benefits of mIAB. Finally, while [10] presents a single taxonomy on fixed IAB, we present a different organization of the reviewed articles. More specifically, different from [10], we highlight that the works do not fit in a unique class of criteria as we classify the same work into different categories and over different perspectives.

Our work is different from [11] from various perspectives. Firstly, while the authors of [11] only focused on moving cells, we also address fixed IAB, which also uses a wireless backhaul. More specifically, we provide an overview of the architecture and protocols standardized by 3GPP to support IAB and, we present a taxonomy for fixed IAB works, which is the basis for mIAB in 5G and beyond 5G. Secondly, [11] only addresses land-based public transport vehicles such as trains, subways, buses, and vans, while we also address cars and UAVs. Finally, as [10], the survey on [11] does not present a detailed performance evaluation on mIAB and does not compare its performance with alternative technologies.

By presenting simulation results that take into account the 3GPP standardized architecture and protocols related to IAB, we aim at comparing the performance of mIAB networks with current networks and at presenting future directions of research to improve its performance.

The present work is organized as follows. First, we present the basis of IAB in Sections II and III. More specifically, Section II presents current IAB aspects already standardized by 3GPP for 5G NR. Besides, Section III presents a literature review of fixed IAB. In this section, the works are classified following different criteria, such as: studied dimensions, system modeling assumptions/constraints, considered problem objectives and key performance indicators (KPIs), solution approaches and adopted mathematical tools.

Furthermore, Section IV presents works related to mIAB. The presented works are first grouped according to the type of mobility, e.g., train, bus, UAV, etc.. This is due to the fact that works considering similar type of mobility usually consider similar problems, e.g., UAV positioning, and take advantage of specific characteristics of each type of mobility, e.g., previously known mobile trajectory of buses. For each type of mobility, we present the most recurrent topics and solutions presented in the literature. Moreover, Section V presents a performance evaluation of mIAB through computational simulations results. Extensive performance analysis is presented, including passengers and pedestrians throughput, latency and link quality in both downlink and uplink transmission directions. Results related to the wireless backhaul are also presented as well as the profile of links served by the IAB donors. Finally, Section VI summarizes the lessons learned and lists some open issues and future directions. Section VII presents the conclusions of this work.

II. IAB ON 3GPP

Wireless backhaul has been studied for years in the literature and the 3GPP has already taken some standardization actions on this matter in the context of long term evolution (LTE) Release 10 [12]. Although wireless backhaul are provided for BSs with the so called LTE relaying [13], the commercial interest on it was not as large as expected. The main limitations of LTE relaying are: 1) limited number of hops, i.e., only single hop is supported; 2) static parent to child architecture; 3) inflexible bandwidth partitioning between access and backhaul; and 4) limited available spectrum [14].

The standardization process on IAB started in 2017 by means of a study item for 5G NR within the scope of Release 15. The technical report [15] describes IAB architectures, radio protocols and physical layer aspects considered by that study item. Later, on July 2020, Release 16 was endorsed, in which protocol layers and architecture of IAB were included in the technical specification [16]. Moreover, the minimum IAB radio frequency (RF) characteristics and minimum NR IAB performance requirements were specified in [17].

Different from LTE relaying, NR-IAB provides greater flexibility by enabling multihop architecture, flexible topology, dynamic resource sharing, as well as the possibility of using mmWave bands for both access and backhaul. Specifically, the wider bandwidths on mmWave together with directionality of massive multiple input multiple output (MIMO) make it possible to use aggressive spectrum reuse and reach higher transmit data rates compared to legacy 6 GHz bands. In the following, we provide more details on IAB architecture and features.

A. IAB Architecture

The integration of IAB in NR strives to reuse existing functions and interfaces. Figure 2 illustrates the IAB architecture adopted in NR. One important aspect is the support of multiple wireless backhaul hops. This is illustrated in Fig. 2a by the blue BSs, called IAB nodes, which can be wireless connected one to another. In contrast, the terminating

gNodeB (gNB), i.e., the gray BS with a wired backhaul and which provides a wireless backhaul to other BSs, is called IAB donor. The IAB NR support of multiple hops helps to overcome two challenges of signal propagation in mmWaves: its limited range of coverage and its low capacity to contour obstacles. However, the main challenges to support multiple hops are related to scalability issues, e.g., increased signaling load and uplink (UL) scheduling latency.

Regarding the IAB nodes, they support gNB distributed unit (DU) and mobile termination (MT) functionalities [16], as illustrated in Fig. 2b. On the one hand, the MT part of an IAB node manages the radio interface layers of its backhaul towards an upstream IAB donor or other IAB node. On the other hand, the DU part provides the NR interface to UEs and to MT parts of downstream IAB nodes.

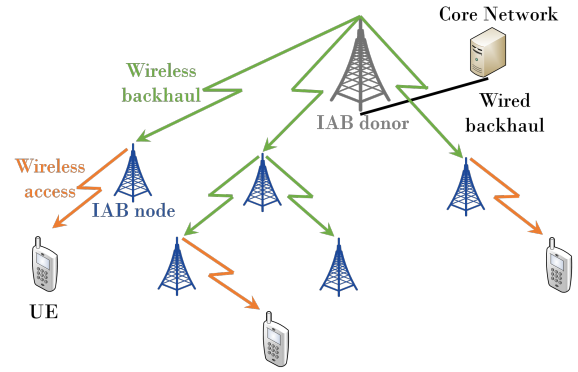
For compatibility purposes with legacy networks, the MT part of an IAB node acts as a regular UE from the point-of-view of its serving BS (either an IAB donor or another IAB node). From a UE point of view, the DU part of an IAB node looks like as the DU of a regular gNB.

Concerning the IAB donor, it is split in centralized units (CUs) and DUs [16]. This split is transparent to the served nodes and these units can be either collocated or non-collocated. As illustrated in Fig. 3, the DUs are responsible for lower protocol layers, e.g., physical (PHY), medium access control (MAC), and radio link control (RLC), while the CUs provide upper protocol layers, e.g., packet data convergence protocol (PDCP) and service data adaptation protocol (SDAP) / radio resource control (RRC). The main objective of this split is to allow time-critical functionalities, e.g., scheduling and retransmission, to be performed in DUs closer to the served nodes, while other functionalities can be performed in CUs with better processing capacity [18].

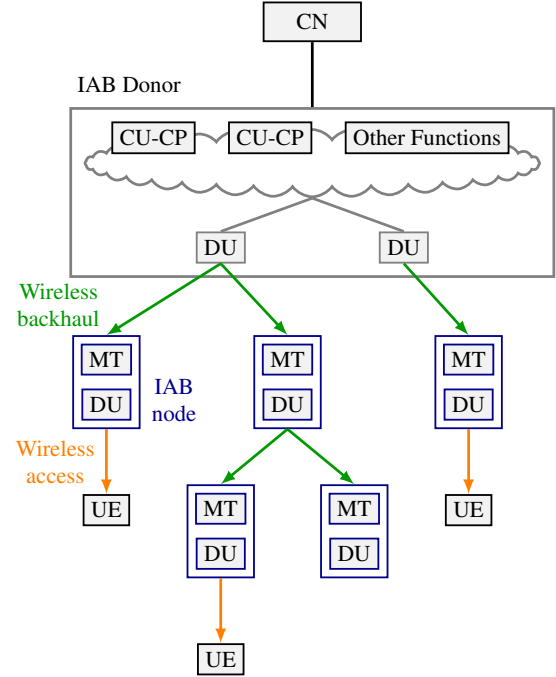
B. Protocol Layers

As it can be seen in Figure 3, CU and DUs are connected via the F1 interface. The open and point-to-point F1 interface supports both the exchange of signaling information by means of F1-C (control plane), and data transmission between end points through F1-U (user plane) [19]. The main capabilities of F1 interface are the management of radio bearers and backhaul RLC channels as well as the transfer of RRC messages between UE and gNB-CU.

According to [15], IAB backhaul can operate in both in-band and out-of-band scenarios with respect to access links. In in-band mode, there is at least a partial overlap between the used frequency resources by backhaul and access links. However, in this case, IAB nodes cannot transmit and receive at the same time in order to avoid self-interference, i.e., they operate in half duplex (HD). So, the DU part of an IAB node cannot transmit while its MT part is receiving and vice versa. In case of in-band scenario, time division multiplexing (TDM) or space-division multiplexing (SDM) should be employed in order to avoid undesirable interferences. In out-of-band mode, the backhaul and access links use different frequency resources so as to avoid cross-tier interference. Time division duplex (TDD) should be employed as NR operators will typically have



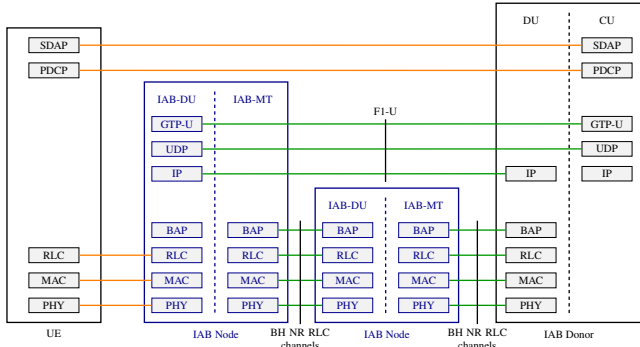
(a) Multiple backhaul hops illustration.



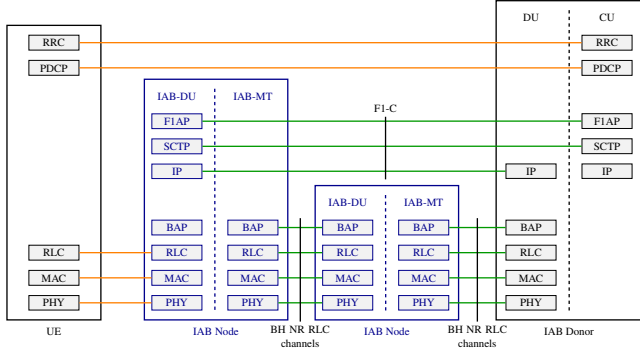
(b) IAB donor and nodes main components.
Fig. 2. IAB NR architecture.

access to wide bandwidth at mmWave. Thus, the time domain should be properly configured to coordinate transmissions in downlink/uplink for access and backhaul links. The time share for uplink/downlink transmissions in access and backhaul to optimize system performance can be based on the system load, for example.

Backhaul RLC or BH NR RLC channels are responsible for transporting traffic between IAB nodes or between IAB donor and IAB nodes. As the functional CU/DU split occurs at RLC layer, IAB nodes are interconnected at this level. Hop-by-hop automatic repeat request (ARQ) is considered for the RLC layer instead of an end-to-end ARQ. The main disadvantages of hop-by-hop ARQ are the higher packet forward latency (due to the RLC-state machine on each hop) and the lack of guarantee for lossless uplink packet delivery in certain scenarios, e.g., topology adaptation due to link failure. However, end-to-end ARQ at RLC layer leads to latency due to retransmissions that increases with the number of hops. Another drawback of end-to-end ARQ is that a packet loss



(a) User plane.



(b) Control plane.

Fig. 3. Protocol stack.

requires retransmission in multiple links including the ones whose transmission was successful [15]. Multiple backhaul RLC channels can be setup on each backhaul link to assure quality of service (QoS) guarantees. More specifically, there are two types of mapping between UE data radio bearers and backhaul RLC channels: one-to-one and multiple-to-one mappings. In the first case, each UE radio bearer is mapped to a separate backhaul RLC channel, whereas in the second case several UE radio bearers are multiplexed onto a single backhaul RLC channel. On the one hand one-to-one mapping can ensure strict QoS guarantees, but on the other hand multiple-to-one mapping decreases the signaling load and required number of RLC channels that should be established.

One of the premises of IAB standardization is to decrease at maximum its impact on NR Release 15 specifications. However, in order to support routing across IAB nodes, i.e., control how packets are forwarded among IAB nodes, IAB donor, and UEs, a new protocol sublayer was proposed: the backhaul adaptation protocol (BAP) [20]. In this sense, the BAP sublayer is responsible for efficient forwarding of internet protocol (IP) packets between IAB nodes on the top of RLC backhaul channels. In downlink, the BAP sublayer of the IAB donor DU encapsulates PDCP packets that, in their turn, are transmitted through RLC backhaul channels and, finally, de-encapsulated at the DU side of the target IAB node. In uplink, the PDCP packets are encapsulated at the IAB node in the origin and de-encapsulated at the DU part of the IAB donor. Each IAB node owns a BAP address that uniquely identifies it in an IAB network. The header of a BAP packet carries a BAP routing identification (ID) that is setup by the

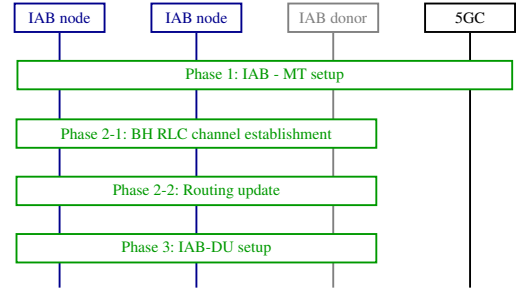


Fig. 4. IAB node integration procedure [21].

CU part of donor IAB. The routing ID is composed of a BAP address and a BAP path ID. While the former identifies the destination node where the packet should be delivered, the latter defines the routing path that the packet should follow, if more than one, until reaching the destination node. Therefore, at each node, the BAP header should be inspected in order to determine if the packet has reached its destination or to determine the next hop that the packet should be forwarded to. In downlink, the DU part of IAB donor is responsible for inserting the header of BAP packets, while in uplink this task is performed by the first IAB node in the route. The routing table used for uplink and downlink can be different from each other.

C. Network Procedures

Regarding integration of new IAB nodes to the system, topology adaptation and IAB resource configuration, 3GPP tried to be as much as possible compatible with legacy procedures and adapted the equivalent procedures of a regular gNB for the case of an IAB node. In the following, we briefly present how these procedures work in the context of IAB.

C.1 IAB Node Integration Procedure

3GPP specified in [21] how a new IAB node is integrated to the system. This procedure is illustrated in Fig. 4 and is split into three phases.

In the first phase, the IAB-MT of the new IAB node connects to the network in the same way as a regular UE with two differences [16]: 1) the IAB-MT ignores cell-barring or cell-reservation indications contained in cell system information broadcast; 2) the IAB-MT only considers a cell as a candidate for cell selection if the cell system information broadcast indicates IAB support. Except for the mentioned differences, the IAB-MT, as a regular UE, searches the frequency band for synchronization signal blocks (SSBs) in order to identify the most suitable cell. After a successful random access, the IAB-MT performs a RRC connection setup procedure with the IAB donor-CU, authentication with the CN, and context management and radio bearer configuration with intermediary IAB nodes, if any.

The second phase is split into two main parts. The first part concerns the establishment of new BH RLC channel or modification of an existing one between the intermediary IAB node and the IAB-donor-DU. This part also includes configuring the BAP Address of intermediary IAB nodes and

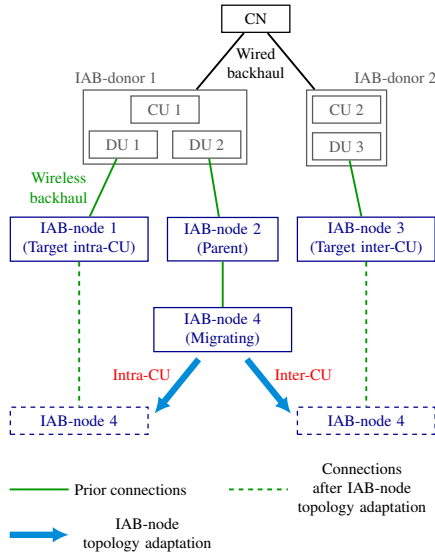


Fig. 5. Topology adaptation illustration.

default BAP Routing ID for the upstream direction. In the second part, the BAP sublayer is updated to support routing between the new IAB node and the IAB-donor-DU.

Finally, the third part concerns the configuration of the DU part of the new IAB node. The F1 link between the IAB donor CU and the DU part of the new IAB node is setup with the allocated IP address. After that, the new IAB node is ready to start serving UEs.

C.2 Topology Adaptation

After being integrated to the system and connected to a parent node, an IAB node may need to migrate to a different parent node, e.g., when the link towards its current parent becomes weak due to mobility or obstacles between transmitter and receiver. For this, topology adaptation is performed.

Figure 5 illustrates an example where IAB node 4 needs to migrate to another parent. Its serving IAB parent (IAB node 2) and the target one (IAB nodes 1 or 3) may be served either by the same IAB donor-CU (intra-CU) or by a different IAB donor-CU (inter-CU). 3GPP defined in [21] different procedures for each case.

In both intra-CU and inter-CU topology adaptation procedures, first the migrating node (IAB node 4) sends a measurement report to its parent node (IAB node 2). This measurement report is forwarded from IAB node 2 towards its IAB-donor CU (CU 1) via an UL RRC transfer. The IAB-donor CU is responsible for evaluating if a topology adaptation is required. If so, it chooses a target node to be the new parent of the migrating node.

If the target node (e.g., IAB-node 1) is served by this IAB-donor CU, i.e., CU 1, (intra-CU topology adaptation), this CU directly sends a message to the target node with a `CONTEXT_SETUP_REQUEST`. If CU 1 receives a positive response, it sends a RRC reconfiguration message to IAB node 2 (the current parent), which forwards this message to IAB node 4. IAB node 4 will then perform

a random access procedure towards the target parent, i.e., IAB node 1. If everything goes well, the new connection is established, and the migrating IAB node sends a `RRC_RECONFIGURATION_COMPLETE` message to its new parent (IAB node 1), which forwards this message to the IAB donor CU. Finally, the BH RLC channels are configured and the BAP route and mapping rules are updated.

Otherwise, if the target node (e.g., IAB-node 3) is served by another IAB-donor CU (e.g., CU 2 in an inter-CU topology adaptation), then CU 1 sends a HO request via X_n interface to CU 2. Similar to the previous case, CU 2 will send a `CONTEXT_SETUP_REQUEST` to the target IAB node 3 and wait for a response and, if it is positive, CU 2 will send a HO ACK to CU 1. Also similar to the previous case, CU 1 then sends a RRC reconfiguration message to IAB node 2 (the current parent), which forwards this message to IAB node 4. IAB node 4 will then perform a random access procedure towards the target parent, i.e., IAB node 3. If everything goes well, the new connection is established, and the migrating IAB node sends a `RRC_RECONFIGURATION_COMPLETE` message to its new parent (IAB node 1), which forwards this message to its IAB donor CU (CU 2). Finally, a new F1 is established between IAB node 4 and CU 2, the BH RLC channels are configured, and the BAP route and mapping rules are updated.

It is worth noting that, for both cases, the parent IAB-node never directly communicates with the target parent IAB-node. The communication between them is performed through the IAB donor CU. Also, according to [21], in upstream direction of intra-CU topology adaptation, in-flight packets between the source parent IAB node and the IAB donor CU can be delivered even after the target path is established, while, in-flight downlink data in the source path may be discarded, since the IAB donor CU can determine unsuccessfully transmitted downlink data over the backhaul link.

C.3 IAB Resource Configuration

The deployment of wireless backhaul is a potential source of interference in the system. In order to avoid self-interference and sometimes due to hardware limitations, in general, IAB-DU and IAB-MT operate in HD, i.e., IAB-DU does not transmit at the same time as IAB-MT receives and vice-versa. However, some special cases of IAB-full duplex (FD) are envisioned, e.g., when the antennas of IAB-DU and IAB-MT point towards different directions or the IAB-MT is outside and the IAB-DU is inside [22].

Regarding the direction (transmission or reception) in which the frequency resources are used in the time domain by an IAB-MT, they can be configured via RRC signaling by the IAB node parent as downlink, uplink or flexible. When configured as downlink, it is only used by the parent in the downlink direction (MT reception only). When configured as uplink, it is only used by the parent in the uplink direction (MT transmission only). When configured as flexible, it can be used in either direction (but not simultaneously). Its instantaneous direction is determined by the parent node scheduler.

Similar to the MT frequency resources, the IAB-DU resources can also be configured as downlink (DU

transmission only), uplink (DU reception only), and flexible. However, another configuration is also allowed for the DU resources: not available. In this case, the DU is not allowed to use that resource at all.

To coordinate the use of resources by IAB-DU and IAB-MT parts, an IAB-DU resource can be configured by the parent node as hard, unavailable or soft [16]. If configured as hard, the IAB-DU can use it no matter if it is used by the IAB-MT. In this case, the parent node should avoid transmitting/receiving to/from the IAB-MT in this resource. If configured as unavailable, it cannot be used by the IAB-DU, except for some special cases. Finally, if configured as soft, the IAB-DU can use it conditionally either on an explicit indication of availability by the parent node or on an implicit determination of availability by the IAB-DU based on whether or not the use of that resource impacts the IAB-MT. It is the CU's responsibility to configure both the parent IAB node and the IAB node such that their respective availability configuration are compatible.

With respect to IAB-MT UL scheduling, increased latency due to multiple hops can adversely impact the system performance. The reason for this is that usually an equipment only requests UL data transmission after it actually receives the data to be transmitted, informed via a buffer status report (BSR). In other words, in a multihop system, the delay is cumulative since an intermediary equipment must first receive the data, before requesting UL resources and finally forwarding the data in UL. To overcome this issue, it was standardized in [16] that an IAB-node can send a pre-emptive BSR to request UL resources, i.e., request UL resources based on expected data rather than on data already buffered. In this case, when data is received by an intermediary IAB node, UL resources are already reserved to be used for forwarding the data to the IAB parent.

D. IAB in Release 17

Due to the restrictions imposed on face-to-face meetings by COVID-19 pandemic, 3GPP has revised the Release 17 timeline. The Release 17 Stage 3 functional freeze is expected to occur on March, 2022. A new work item entitled *Enhancements to Integrated Access and Backhaul for NR* has been approved for Release 17 [23], the main objectives of which are [24]:

- Topology adaptation enhancements and routing: Among the main studies in this topic we can mention the specification of inter-donor IAB migration and reduction of the associated signaling load. The main objectives of this topic are the increase of system robustness and load balancing. Moreover, support for CP/UP separation and reduction of service interruption time, e.g., during IAB-node migration, are also envisioned to increase reliability. Remaining studies are focused on multihop latency and congestion mitigation.
- Duplexing enhancements: HD constraint imposes limitations on IAB operation. In this topic, the focus is to improve spectral efficiency and latency by supporting simultaneous operation of IAB node's child and parent. In this case, it is possible that the MT part of an IAB node

could transmit while the DU part of the same node could be receiving, i.e., FD mode. Another possibility is the simultaneous transmission or reception of MT and DU parts by leveraging spatial multiplexing techniques. Furthermore, dual connectivity scenarios should be considered so as to improve robustness and perform load balancing.

III. OVERVIEW ON FIXED IAB

A. Taxonomy on Fixed IAB

Thanks to the great flexibility of IAB networks, the existing literature on fixed IAB can be categorized over many different criteria. In this section, we provide a taxonomy of the works on IAB according to the following criteria:

- 1) Studied dimensions and article profile: the system performance on IAB networks can be improved by optimizing different aspects. In this criterion, the works can be characterized according to the functionalities that are studied. The considered categories are surveys, overview, testbeds, IAB versus fiber-based network performance, network deployment, routing and topology adaptation, resource allocation for access and/or backhaul, power allocation, UE association, MIMO beamforming;
- 2) System modeling assumptions and constraints: depending on the dimensions that are being optimized in each article, the authors can make some assumptions about the system model that can boost performance gains but, at the same time, can turn the problems harder to solve. In this criterion, we consider the following categories: FD, intelligent reflecting surface (IRS), multihop, multiple antennas, UE-centric approach, modeling of both uplink and downlink, modeling of access and backhaul links, mesh topology and non-orthogonal multiple access (NOMA);
- 3) Problem objectives and KPIs: the performance of IAB networks can be measured over different points of view, therefore, different objectives and metrics are optimized in the reviewed articles. In this criterion, we assume the following categories: fairness, latency, spectral efficiency, energy efficiency, data rate guarantees for UEs, coverage probability, weighted sum rate, and symbol error rate;
- 4) Solution approaches and mathematical tools: in this criterion, the works can be classified according to the employed tool in order to solve the studied problem(s). Among the common tools we can mention: convex optimization, linear (continuous) optimization, integer linear optimization, heuristics, dynamic programming, machine learning and metaheuristics, stochastic optimization, game theory, stochastic geometry, and statistical analysis.

Note that, depending on the assumed criteria, the same work can be classified in more than one category. In the following section, we describe some important works on fixed IAB clearly identifying the classification according to the established criteria.

B. Literature Review on Fixed IAB

In Figure 6, we present the taxonomy for the reviewed articles in fixed IAB assuming the four abovementioned criteria. For the sake of organization, the works are presented in the following according to the first criterion.

B.1 Surveys, Overview Papers, Testbeds, and IAB versus Fiber-Based Network Performance

The works [10], [14], [18], [25]–[31] provided an overview of IAB technology by describing several aspects regarding architecture, protocol aspects and/or physical layer. More specifically, [10] provides a survey on fixed IAB. Its authors classified IAB works in the following groups: stochastic geometry-based works, resource allocation, scheduling, cache-enabled IAB networks, optical IAB networks and non-terrestrial IAB networks. The works [26], [28] presented a proof of concept of a two-hop IAB network using two-sectors IAB nodes operating at mmWave. In [31], a testbed was presented composed of a donor BS, an IAB node and a UE. The works [26], [28], [31] demonstrated the potential of IAB in a practical setup.

The works [14], [18] as well as [30], [32]–[34] presented simulation results of IAB networks versus fiber-based networks. Some of the conclusions that can be gathered from those works is that IAB performance is close to the one of all-wired networks for low and moderate traffic, and that the performance of fully-fiber connected networks can be achieved with a small increase in the number of IAB nodes in IAB networks. Moreover, they showed that IAB is a relevant technology for 5G since it allows to incrementally improve the fiber density in the network.

B.2 Network Deployment, Routing and Topology Adaptation

Network deployment, routing and topology adaptation were studied in [14], [27], [33], [35]–[48]. In general, for a broad range of coverage constraints/blockage densities, the impact of meshed communication to increase redundancy may be negligible if the network is well planned. In [33] the authors studied a convex optimization problem with the objective of maximizing the product of UEs' downlink and uplink data rates (geometric mean) subject to capacity and resource allocation constraints. Two IAB topologies were considered: mesh and spanning tree based on highest channel quality among IAB nodes. Simulation results showed that the presented mesh topology improved data rate fairness slightly.

In [38] the authors studied a downlink backhaul optimization problem to maximize the minimum data rate among nodes (access links were not considered). An alternative formulation was also presented with the objective of penalizing higher delays in order to induce the use of fewer hops. The routing problems were solved by using linear optimization techniques. The main conclusions obtained from the simulation results were the relevance of taking into account the directional interference among nodes, and that routing complexity can be decreased by splitting the nodes into independent clusters and solving the optimization problem separately for each cluster. In [37], the authors

extended their own work in [38]. In this work, the authors revisited the problem in [38] where the problem size increases exponentially with the number of links, and provided a new scalable formulation that scales near linearly with the number of links.

In [41] the authors studied routing and power allocation for a multihop IAB network with FD BSs employing hybrid beamforming. A utility maximization problem was formulated subject to constraints on the delay violation probability and queue stability. A routing subproblem was solved by employing reinforcement learning (RL). In the results, the authors highlighted the relevance of the path selection functionality in order to assure higher reliability and lower latency. Improved latency and better throughput were reported by [42] where resource allocation for access/backhaul, power allocation and a dynamic routing (based on real network traffic) were studied.

Mesh topology was studied in [44] for IAB networks. The authors proposed a mesh topology for IAB networks where the split DU/MT in IAB nodes is replaced by a peer unit. Each peer unit of an IAB node can be dynamically configured as master or slave. An IAB node configured as master can control their links to other IAB nodes configured as slaves as well as its own access links. Simulation results showed that the proposed mesh topology provides lower packet delays and significant total throughput gains for bursty traffic when compared to classical topologies. Mesh networks for IAB was also studied in [43] where the authors studied the problem of maximizing the number of delivered broadcast packets. Optimal and suboptimal solutions were proposed. Mesh IAB with IRSs was studied in [47]. The authors reported that the use of IRS is capable of improving signal to noise ratio (SNR) and symbol error rate (SER), which allows for the use of higher modulation orders, and that outage probability for multiple hops can be reduced if the number of elements in IRS is increased. However, it is important to highlight that none of the works presented in this section about mesh topology included in their analysis the increased complexity of enabling a mesh architecture in IAB networks in terms of signaling overhead, for example.

The authors in [45] considered a heterogeneous network and studied the problems of power allocation and routing. In this work, they assumed cooperation between BSs that can employ orthogonal multiple access (OMA) and NOMA multiple access schemes. The main outcome of this work was the proposal a joint and adaptive greedy routing solution that switches between cooperative OMA and NOMA in order to maximize energy efficiency subject to data rate and power constraints.

In [36], the authors studied distributed routing strategies (path selection) for IAB networks. Four routing solutions were presented: highest-quality-first, wired-first, position-aware and maximum-local-rate policies. In highest-quality-first solution, the next hop is the one that presents the highest signal to interference-plus-noise ratio (SINR) whereas in wired-first one, the chosen hop is the one that provides the shortest path to the IAB donor. The main idea in position-aware policy is to achieve a balance between highest-quality-first and wired-first

Criteria for taxonomy	Categories	Works
Studied dimensions and article profile	IAB overview	[10], [14], [18], [25]–[31]
	IAB performance versus fiber	[14], [18], [30], [32]–[34]
	Survey	[10]
	Testbeds	[26], [28], [31]
	Network deployment, routing and topology adaptation	[14], [27], [33], [35]–[48], [57]
	Resource allocation for access and/or backhaul	[18], [34], [39], [42], [46], [48]–[58]
	Power allocation	[41], [42], [45], [46], [51], [53], [54], [59]
	MIMO beamforming	[29], [51], [60]–[63]
	UE association	[34], [46], [51], [60]
System modeling assumptions and constraints	Full duplex nodes	[29], [41], [42], [45], [53], [55], [60], [63]
	IRS	[47]
	Multihop	[14], [28], [30], [33], [35]–[38], [40]–[48], [52], [56]–[58]
	Multiple antennas at IAB nodes	[14], [18], [27]–[31], [33], [35]–[39], [41], [42], [46], [48], [51], [56], [60]–[63]
	User-centric approach	[33], [40], [41], [51], [60]
	Uplink and downlink modeling	[30], [31], [33], [37], [42], [44], [56], [62]
	Access and backhaul links modeling	[14], [18], [28]–[36], [41], [42], [44], [46]–[56], [58], [60], [62], [63]
	Mesh topology	[33], [37], [38], [43], [44], [47], [52]
	NOMA	[45], [54]
Problem objectives and KPIs	Fairness	[33], [37], [38], [41], [48], [51]–[53], [55]
	Latency	[14], [32], [35]–[37], [39], [41]–[44], [56]
	Spectral efficiency	[28], [29], [32], [35], [36], [40], [42]–[44], [57], [61], [63]
	Energy efficiency	[45], [54]
	Data rate guarantees or UEs	[14], [30], [54], [56], [58]
	Coverage probability	[18], [27], [31], [34], [47], [49], [50], [59], [62]
	Weighted sum rate	[46], [51], [60]
	Symbol error rate	[47], [63]
Solution approaches and mathematical tools	Convex optimization	[33], [41], [43], [46], [51]–[54], [60], [61]
	Linear (continuous) optimization	[37]–[39], [48], [57]
	Integer linear optimization	[37], [39]
	Heuristics	[14], [28]–[32], [35], [36], [40], [42], [44]–[46], [48], [51], [56], [60], [62], [63]
	Dynamic programming	[40], [43], [58]
	Machine learning and metaheuristics	[27], [41], [55], [59]
	Stochastic optimization	[41], [60]
	Game theory	[52]
	Stochastic geometry	[18], [27], [34], [49], [50]
	Statistical analysis	[47]

Fig. 6. Taxonomy for fixed IAB: studied dimensions and article profile, system modeling assumptions and constraints, problem objectives and KPIs, and solution approaches and mathematical tools.

solutions. Finally, the maximum-local-rate solution chooses the next hop with highest data rate that, in its turn, takes into account the number of connected UEs in the parent IAB node, i.e., IAB load. Performance results showed that wired-first policy provided a reduced number of hops at the cost of lower worst-SINR while the best performance for low-SINR regime was achieved by position-aware policy. Similar routing solutions and some new variants were evaluated in [14], [35]. In [14], the authors showed that choosing wired-first routing instead of highest-quality-first provides higher throughput and lower latency. In [35], the reported results showed that although highest-quality-first routing improved the link quality at backhaul and access links, the number of hops to the core network has increased. Strategies based on path data rate, i.e., end-to-end data rate, were able to reduce the number of hops to the core network.

A heterogeneous network was assumed in [39] where resource allocation and routing were studied for a two-hop IAB network. A mixed integer optimization problem was formulated to minimize the makespan, i.e., the time needed to deliver all packets from macro BS to the small BSs. Based on analytical insights, the authors proposed a heuristic solution to the formulated problem. The simulation results showed that the makespan increases with the average file and network sizes.

In [46], the authors assumed a multihop IAB network and studied the problems of resource allocation, user association, power allocation as well as IAB node positioning. Focusing on the IAB node positioning problem, long-term channel statistics, UE density and UE-BS association were considered as input to optimize node placement. The objective was to maximize weighted sum rate and closed-form solutions were developed for node positioning assuming distributions related to the probability of a UE getting assigned resources. The proposed node positioning showed to be efficient when compared to exhaustive search solutions.

Topology formation and adaptation for IAB networks were evaluated in [40]. Optimal and suboptimal solutions were proposed for a topology formation problem that maximizes the minimum capacity along the system. As conclusion, they showed that for few IAB nodes, all algorithms achieved a similar performance since the number of options for topology formation is not high.

In [27], the authors assumed an IAB network where there are IAB donors and small BSs where two problems were studied: small BS positioning and decision if a small BS should be directly connected to the core network (small BS to donor assignment). The results showed that the optimization of IAB node positioning and small BS to donor assignment outperform random positioning. Finally, the authors showed that network planning decreased the need of routing updates during temporal link blocking.

Resource allocation and routing were the focus of [48] by assuming a time division multiple access (TDMA)-based multihop IAB network. An optimization problem of maximizing the minimum node's throughput was formulated subject to time resource constraints. Both routing and resource allocation were jointly solved by applying an iterative solution based on Simplex and maximum matching

theories. Simulation results showed that the minimum node's throughput is increased as the number of macro and small BSs increases as a result of shorter link distances and decreased number of backhaul hops.

B.3 Resource Allocation for Access and/or Backhaul

As opposed to out-band operation where the access and backhaul operate in different frequencies, in-band backhauling refers to the cases with the access and backhauling sharing the same resources. Compared to out-band backhauling, in-band operation leads to higher flexibility at the cost of complexity. The state-of-the-art works concentrate mainly on in-band backhauling [18], [34], [39], [42], [46], [48]–[55].

In [49] the authors employed stochastic geometry to model a two-hop heterogeneous IAB network. The total mmWave bandwidth is partitioned into two parts: the first for backhaul and the second for access. The access bandwidth is shared among UEs in a round-robin fashion. On the other hand, there are two options on how the backhaul bandwidth is shared among IAB nodes: equal partitioning and instantaneous load-based partitioning. In the equal partitioning strategy, the bandwidth is equally split among IAB nodes. In the instantaneous load-based strategy, the allocated bandwidth is proportional to the current load on each IAB node. Simulation results showed that load-based partitioning outperforms the equal partitioning at the cost of a high signaling rate. In [18], the authors studied a similar problem involving bandwidth partitioning between access and backhaul based on a fixed split factor.

In order to reduce signaling load, in [50], a load-based resource partitioning among IAB nodes was proposed. Here, the load reported by IAB nodes is averaged over long intervals. In the simulation results, the authors showed that the average load-based partitioning achieves a good performance-signaling load trade-off.

The work [34] is an extension of [49]. The bandwidth split between access and backhaul based on a fixed factor proposed in [49] is called orthogonal resource allocation (ORA) in [34]. In this work, the authors proposed an alternative solution called integrated resource allocation (IRA) where the bandwidth assigned by a donor IAB to the backhaul for a given IAB node depends on the access load of the IAB node. Simulation results showed that the coverage probability in ORA is highly dependent on the bandwidth split factor. As the number of small BSs increases, more bandwidth should be reserved to backhaul in ORA scheme. Coverage probability provided by IRA is better than the one achieved with the static ORA scheme.

In [51], the problems of user association, hybrid beamforming design, power allocation and resource allocation were studied. A weighted sum rate maximization problem with limited channel state information (CSI) was formulated. Due to the complexity of the formulated problem, the authors followed a two-stage approach. At stage 1, user association and beamforming are designed for access links. After that, in stage 2, the decisions for access links are signaled to the macro BS that in its turn solves resource allocation and beamforming problems for backhaul links. Simulation results showed that

the time fraction assigned to access links increases as a result of higher transmit power at macro BS. On the other hand, the increase of the transmit power of small BSs results in a lower time fraction for access links.

Resource allocation was studied in [52] for a mesh network that combines the concepts of IAB and user provided network (UPN) where high channel quality UEs are capable of relay information towards bad channel quality UEs. A Nash bargaining solution was proposed to solve the resource sharing problem among concurrent links as well as to define how UEs and the operator should cooperate. Simulation results showed that the proposed cooperation scheme for UPN and resource allocation for IAB resulted in higher network throughput compared to baseline schemes without UPN or resource allocation.

As previously described, resource allocation for access and backhaul was also studied in [42]. In this work, the resource allocation subproblem took the form of defining the spatial multiplexing for the links, i.e., space-division multiple access (SDMA) groups, and the number of slots from the frame assigned to each group. SDMA groups were chosen by using a greedy algorithm based on graph theory. The definition of the number of slots followed a proportional fair policy. In the simulation results, the authors showed that the proposed scheme is more robust than baseline solutions when the number of UEs is increased thanks to the spatial multiplexing capacity.

In [53] the authors assumed a two-hop IAB network with FD-capable nodes. In this work resource allocation for access and backhaul as well as power allocation were studied with the objective of maximizing proportional fairness. Due to the complexity of the formulated problem, the authors resorted to a two-level approach by decomposing the original problem into two problems: backhaul bandwidth allocation and power allocation. The authors showed that the bandwidth allocation is a convex subproblem whose solution can be found in closed form. In the simulation results, the authors evaluated the impact of the density of connected UEs to donor IAB and IAB nodes on the bandwidth allocation.

Bandwidth and power allocation were studied in [54] for a heterogeneous network with wireless backhaul where the macro BS was equipped with massive MIMO and small BSs employed NOMA in access transmissions. A suboptimal solution for the optimization problem of maximizing the energy efficiency of the small BSs subject to minimum UE data rate guarantees was formulated. In the simulation results, the authors showed that there is a specific bandwidth partitioning that leads to the optimal energy efficiency.

Downlink subchannel allocation for access and backhaul in a two-hop IAB network was studied in [55]. The nodes are assumed to be FD-capable and a single antenna is assumed for DU and MT parts. An optimization problem was formulated with the objective of maximizing a utility function (later set to proportional fairness) subject to data rate guarantees for UEs. A learning-based solution was proposed and, according to simulation results, it outperformed the static full-reuse solution in terms of fairness.

Besides studying routing problems as previously described,

the authors in [39] developed a model for resource allocation in backhaul transmissions. The fraction of the capacity of each active link to transmit data to small BSs was also optimized to minimize the makespan. One important assumption in this work is that the interference pattern among nodes is known to the macro BS or IAB donor.

Considering multihop IAB networks, [46] develops bandwidth allocation schemes for access and backhaul. In this work, the authors assumed that orthogonal bands are assigned to each backhaul and access link. In a centralized operation, where most of the resource allocation decisions are taken on IAB donors based on channel quality information sent from child nodes, channel aging should be taken into account. Channel aging is caused by the fact that the channel quality estimate used by donor IAB may change considerably when resource allocation decisions are actually employed by child nodes. A subcarrier allocation problem is formulated within each band with the objective of maximizing the weighted downlink spectral efficiency. The simulation results showed that channel prediction together with efficient resource allocation lead to a good performance when channel aging and low-mobility UEs are assumed.

The work [48] studied both routing and resource allocation for access/backhaul in a multihop TDMA-based IAB network as detailed in Section III-B2. Focusing on the resource allocation problem, the authors assumed that a frame is divided into a number of time slots with variable lengths. The formulated problem has the objective of maximizing the minimum nodes's throughput (fairness). The proposed scheme outperforms the macro-only scenario over different conditions.

In [56], the authors focus on how scheduling, i.e., resource allocation, can be performed in a semi-centralized architecture. In IAB networks, the scheduling decisions for access links associated with a given node, e.g., IAB donor or IAB node, are in charge of its local DU. Thus, essentially, the proper association among time-frequency resources and links is a distributed task among network nodes. This assumption was not followed by some of the previous described works, such as [39], [42], [46], [48] where centralized solutions were proposed.

Specifically, in [46], the authors showed that the performance gains of centralized solutions is strongly dependent on the effect of channel aging. Although fully centralized scheduling is not 3GPP compliant for IAB, nodes can exchange information and eventually, it can be assembled in a central node where general recommendations for resource allocation and scheduling can be informed to the other network nodes. This is the key idea of [56]. In this work, a central controller receives general information about network nodes, e.g., CSI and buffer status, and provides centralized recommendations for resource partitioning to the distributed schedulers. However, the local DUs are free to follow or not the indications of the central controller depending on local conditions. One important conclusion of this work is that this semi-centralized framework provides performance gains, however, it strongly depends on the capacity of the system in exchanging information in a timely manner.

The previous described works [18], [34], [49]–[51] present

resource allocation and scheduling solutions that can be classified as a semi-centralized operation where partitioning of bandwidth between access and backhaul is taken in a central node based on the available system information, but the proper association among system resources and links are decided locally.

In [57], the authors proposed a distributed/decentralized solution to scheduling/resource allocation problem. The proposed solution takes advantage of the information spread by network nodes about the bandwidth allocated to their children as well as the local perspective obtained about network topology. Based on this information, local optimization problems are solved at each node for resource allocation.

Finally, in [58] the authors proposed distributed schedulers for multihop IAB assuming a limited number of RF chains. An optimal back-pressure scheduling solution as well as a distributed message passing scheme were proposed in order to achieve queue stability. Furthermore, another contribution of [58] was the proposal of local schedulers with a simplified exchanging of messages between nodes.

B.4 Power Allocation

Power allocation may be useful for the cases with simultaneous operation at the IAB node, especially if the network deployment is not well planned. For this reason, power allocation has been discussed in 3GPP Release 17 work-item on IAB enhancements. Power allocation was also studied in [41], [42], [45], [46], [51], [53], [54]. With exception of [59], it is important to note that power allocation was not studied alone in those works; in fact, power allocation was jointly studied with resource allocation for access and/or backhaul, routing/topology adaptation or UE association. Routing and power allocation was studied in [41]. The main outcome of this work was that power allocation leads to only marginal improvements in the delay performance when intelligent routing is already considered. Power allocation for SDMA groups and assuming fixed routing was also studied in [42] with the objective of maximizing spectral efficiency.

Besides user association and resource allocation, power allocation problem was studied in [51]. Hybrid beamforming was assumed in this work. Therefore, the power allocation problem for downlink was studied together with the baseband beamforming design for access and backhaul links. In the simulation results, the authors showed the effect of the available power at macro and small BSs on the total data rate and time share for access transmissions. As expected, the time share for access transmissions increases as the power of macro BS increases and/or the power at small BSs decreases.

In [53], the authors decoupled the original optimization problem in resource (bandwidth) allocation and power allocation for maximizing the proportional fairness in the system. After solving bandwidth allocation, the transmit power allocation for downlink was solved for access and backhaul independently since there is no coupled constraints. From the simulation results, the authors showed that throughput can be increased until a certain level as the downlink access transmission power is augmented. For higher access

transmission power, the backhaul capacity starts to limit the UEs' data rates.

Besides bandwidth allocation, as previously described, power allocation was studied in [54] with the objective of maximizing energy efficiency. The bandwidth and power allocation original problem for downlink was solved by leveraging fractional programming properties and sequential convex approximation. The authors showed in the simulation results that energy efficiency increases with the macro BS's transmit power, however, the high transmit power at small BSs leads to a higher power consumption per data rate which results in poor energy efficiency.

In [45], the authors studied routing and power allocation for downlink by proposing a joint cooperative OMA and NOMA scheme, as previously described in Section III-B2. For the proposed and baseline schemes, power allocation for each small BS was analytically defined so as to ensure minimum data rate guarantees for backhaul links. Simulation results showed that, as the number of relaying small BSs is gradually increased, the performance of cooperative OMA and NOMA in terms of energy efficiency and power consumption is improved until a certain point. Moreover, results showed that joint cooperative OMA and NOMA enjoys the benefits of both cooperative OMA and NOMA and presents better performance in different conditions.

Joint power allocation and subcarrier assignment for downlink were considered in [46] for a multihop IAB network. As different subbands were assigned to each backhaul link and access, power allocation was optimally derived for subcarriers within each subband. Suboptimal power allocation solutions were also provided, which showed negligible performance loss to the optimal solutions according to simulation results.

In [59], uplink power control for dual-hop IAB networks was studied. The main objective of the power control solution was to maximize the coverage probability by employing genetic algorithm (GA). By simulation results, the authors showed that power control is able to substantially improve the coverage probability especially when out-of-band IAB is used. Also, the authors showed that inter-cell interference does not play an important role since mmWave band was assumed and, thus, signal strength quickly decreases with distance.

B.5 MIMO, Beamforming and UE Association

The impact of UE association is considerably different in IAB networks when compared to conventional fiber-based networks. The main reason is that the load of UEs transferred from donor IAB to IAB nodes comes back to IAB donors through the backhaul. Thus, UE association and load balancing should be re-thought for IAB networks. Moreover, multiple antennas technology, that is a key aspect for 5G, assumes a relevant role in IAB networks since backhaul data rates should be in the order of the total access data rate of IAB nodes. Spatial multiplexing between access and backhaul links is also another aspect that has the potential to increase IAB efficiency. In the following, we present some important works related to this topic.

The proper connection between UEs and BSs, i.e., UE association, was investigated in [34], [46], [51], [60]. In [34],

the criterion to define which BS a UE should connect to is based on the highest product between the received power and a constant bias. In the simulation results, the authors showed that, as the bias factor of IAB nodes increases relative to the one of IAB donors, more UEs are offloaded to the IAB nodes, thus increasing the load in backhaul links.

The work [51] studied resource allocation and power allocation, as previously described. Furthermore, the transmitting RF beams of small BSs and the receiving RF beams of the UEs were optimized using analog beamforming. In order to solve the baseband beamforming of small BSs, the weighted maximization problem was converted to a signal to leakage-plus-noise ratio (SLNR) problem in order to reduce the complexity. Once access links were designed, beamforming for backhaul links should be designed. RF beamforming was defined based on the steering beamforming vectors for the line-of-sight directions of the active small BSs. Then, baseband beamforming was found by solving an SINR balancing optimization problem. In the simulation results, the proposed hybrid beamforming based solution outperformed baseline solutions for full-CSI and achieved an acceptable performance degradation compared to the fully digital beamforming solution.

UE association and beamforming were studied for downlink in [60] in a user-centric approach where a UE is served by a group of small BSs (cluster). Small BSs, in their turn, receive data intended to the UEs by means of multicast transmissions from macro BSs. The authors formulated an optimization problem for maximizing the weighted UE data rate under perfect CSI through joint design of multicast beamforming at backhaul, access beamforming and small BS clustering subject to power constraints at small and macro BSs. A heuristic solution was proposed to solve the beamforming design and clustering problems. From the simulation results, for the perfect CSI and static clustering assumptions, the authors showed that the proposed solution outperformed baseline solutions especially for large available power at macro BS.

In [61], the authors focused on MIMO for backhaul links. The expected spectral efficiency for wireless MIMO backhaul links is much higher than in MIMO access links. Therefore, physical impairments such as time offset, which can lead to inter symbol interference (ISI), and phase noise that increases the multi-access interference due to outdated precoder and decorrelator should be carefully mitigated for backhaul links. The main contributions of the article were the proposal of a time offset compensation, phase noise estimation and design of a precoder/decorrelator. In [46], besides studying other problems such as power/bandwidth allocation and node placement, the authors studied UE association. The authors showed that UE association based on average received power may lead to load imbalance. Thus, a load-balancing-based UE association was proposed.

In [62], the authors investigated the impact of the arrangement of antennas in tri-sectorized IAB nodes. In order to decrease inter-sector interference and allow the reuse of frequency resources in different sectors of the same IAB node, two strategies are employed: spatial and angular diversities. In the first one, the arrays of antennas of each sector are disposed

in the vertices of an equilateral triangle whereas the IAB node equipment are located in the center of mass of the triangle. In the second strategy, a minimum angular separation should be kept between UEs associated to adjacent sectors of the same IAB node.

FD-IAB nodes with subarray-based hybrid beamforming scheme was considered in [29]. By assuming that antenna isolation and RF cancellation are perfect, the authors designed digital filters to mitigate residual self-interference (with minimum mean square error (MMSE) combiner) at the IAB receiver and multi-user interference at transmitter (with zero-forcing (ZF) precoder). The proposed scheme is evaluated through simulations by varying channel estimation errors and RF insertion losses, i.e., losses in phase shifters, power dividers and power combiners in mmWave. Simulation results showed the spectral efficiency gains of FD versus HD IAB transceivers as well as showed that the proposed scheme experiences less RF insertion loss than the fully-connected hybrid beamforming. However, it is important to highlight that the actual implementation of FD technology in IAB nodes is still very challenging especially due to self-interference issues. In [63], a further study of the same authors from [29], they assumed a fiber Bragg grating-based analog canceler that is placed before RF precoding and after RF combiner. Reduced bit error rate (BER) were observed in the simulation results when compared to baseline schemes.

IV. MOBILE IAB

Wireless backhaul may allow the deployment of mobile cells, i.e., mIAB, which can hopefully provide uninterrupted cellular services for moving UEs, e.g., passengers in trains and buses.

The concept of mobile cells is not new. Mobile relay nodes (MRNs) were already studied in the past with a similar purpose. It has even been addressed by 3GPP Release 12 in [64]. The focus of [64] was on high speed trains with known trajectory. In the considered topology, outer antennas of access devices, e.g., installed on the top of the train, provide wireless backhaul connection via the evolved node Bs (eNBs) mounted along the railway, while inner antennas installed inside are responsible for providing wireless connectivity to the passengers. Important to highlight that these devices support multi-radio access technology (RAT) functionalities. It means that, while the backhaul link works over LTE, the access link can be deployed over other technologies, e.g., wireless fidelity (Wi-Fi).

A recent technical report from 3GPP [65] presents a study on several use cases and requirements for 5G networks for mobile BS relays mounted on vehicles, i.e., vehicle-mounted relays (VMRs). The study item is part of initial studies for Release 18. The use cases cover many aspects including service provision for both onboard UEs and UEs in the vicinity of the vehicle as well as seamless connectivity in different scenarios involving mobility of UEs and relays.

On the one hand, considering access and backhaul links operating either in different frequency spectrum or even in different technologies simplifies two of the main challenges

related to wireless backhaul and moving cells: managing the resources between access and backhaul links and dealing with the dynamic interference between moving cells and crossed fixed cells. On the other hand, using the same technology and frequency spectrum for both access and backhaul links may result in efficient system operation and optimized use of the scarce and expensive frequency spectrum, respectively.

Next subsection presents a literature review of the main topics related to mIAB.

A. Literature Review

Works related to mIAB, moving relays and moving cells mobile IAB can be classified according to different criteria. Fig. 7 presents the classification adopted in the present survey. The works are first grouped according to the type of mobility, e.g., train, bus, UAV, etc.. This is due to fact that, on the one hand, works considering similar type of mobility usually consider similar problems, e.g., UAV positioning, and take advantage of specific characteristics of each type of mobility, e.g., previously known mobile trajectory of buses. On the other hand, works considering different types of mobility usually consider different environments, e.g., while bus related works try to improve in-vehicle UEs QoS taking into account the presence of out-of-vehicle UEs, train related works only consider the presence of in-vehicle UEs. For each type of mobility, we present the most recurrent topics and solutions present in the literature.

A.1 Train

We start presenting works related to mobile cells deployed at trains. This is a typical use case. Due to the high speed and shielding effect of the trains, it is challenging to continuously serve onboard UEs from outside BSs. With the purpose of reducing the penetration losses caused by the Faraday cage characteristics of a high-speed railway (HSR), state-of-the-art works, e.g. [66]–[70], usually consider that the MRNs are deployed on top of the carriages and connected to in-cabin wireless access points (APs). The MRNs communicate with BSs, playing the role of forwarding data between the passengers on the train and the broadband wireless networks. Furthermore, since the trains follow a predefined track and pass through uninhabited areas, a common solution is to deploy the external BSs along the railway.

Works [66], [67], [71] provide a review on communication on HSR. The authors of [66], summarized key challenges and provided a review of techniques used to address the listed challenges. They focused primarily on physical layer operations covering the rapidly time-varying channel modeling, estimation of fast time-varying fading channels, Doppler diversity transmissions and non-coherent detections. However, they also presented additional discussions on higher layer operations, e.g., handover management, control/user-plane decoupling and network architecture. One of the discussed architectures is the one deploying relays on the roof connected to access points installed inside the train through wired links, such as optical fiber. The MRNs act as intermediate nodes between inside UEs and external

BSs. The authors stated that, since the MRNs are installed outside of the trains, they eliminate the penetration loss. In addition, they usually have LOS with the eNBs. Furthermore, it was highlighted that MRNs can also solve the problem of a high number of simultaneous HO requests, since the HO is performed only between an MRN and an eNB, instead of between multiple UEs and a eNB. That paper did not present either results or more details about the deployment of the MRNs, e.g., central frequency carrier.

In [67], current trends of wireless communications for smart railways were presented. Besides of state-of-the-art, key challenges and issues, the authors also proposed a network slicing architecture for a 5G-based HSR. Similar to [66], in the proposed architecture, APs on the train aggregated the data from different UEs, and relayed them to external BSs through a wireless backhaul. The authors presented simulation results comparing a MIMO-BS-only architecture with the wireless backhaul architecture. However, the simulated scenario was simplified. The train traveled a small distance, less than 10 times its length, and there was only one MIMO-BS positioned in the middle of the path. They assumed a ZF algorithm to reduce the interference caused by inter-UE and inter-AP communications. The simulations showed that the data rate of the mobile wireless backhaul architecture was higher than that of the MIMO-BS-only architecture. They highlighted that, for velocities larger than 360 km/h, it is a challenging task to deploy APs on the train or along the track to make a seamlessly connected heterogeneous network and establish a UE association model for service provisioning. They also remarked that although mmWave shows higher directionality, and thus can be used with more directional antennas making it easier to use mmWave simultaneously for mobile access and backhaul, the specifics of the orthogonalization between these two types of transmissions still need to be further studied.

In [72], the authors advocate that IAB nodes are potential candidates to improve service continuity. For this, they used real measurement from Gangneung Line in a simulated environment to advocate that IAB nodes should be installed in regions where the signal of LTE and LTE railway (LTE-R) are weak in order to avoid radio link failures (RLFs). According to their results, IAB can improve service reliability by 10%, in average. The work [71] describes the main characteristics and requirements for critical and non-critical communications in railways that must be addressed by 5G. The authors highlighted the shielding effect of the train to radio signals, due to its metallic construction. They mentioned that this effect has been quantified in 20-30 dB and therefore, it is necessary to use moving cells for internal network provisioning of reliable communications. They also highlighted the importance of using satellites since high speed lines can travel across large uninhabited areas. Therefore, the trains must be equipped with antennas with mechanical or electrical control of azimuth and elevation.

In [68], [73] results from real measurements are presented. In [73], the authors presented an overview of field trials to assess technical and operating conditions of a 5G mobile communication system capable of supporting high-speed 2 Gbps throughput for HSR. The trials were performed on

Transport Type	Main Topic	Out-of-Band (or not mentioned)	In-Band
General		[11], [64]	
Train	Overall System	[66], [71], [72]	[67]
	Field Trial	[68]	[73]
	Power Allocation	[69]	
	Power Allocation Handover	[70]	
	Beamforming design	[74]	
Vehicular	Channel Estimation	[75]–[78]	
	Probability of Outage		[79], [80]
	Energy Efficiency	[82]	[81]
	Resource Allocation		[83]
	Interference Management		[88]
	Resource Allocation Interference Management		[84], [85]
Bus	Interference Management Resource Allocation	[89]–[93]	[86]
	Interference Management Resource Allocation Power Allocation		[87]
	Handover	[96]	[95]
	Handover Bandwidth Allocation	[94]	
UAV	General	[97]	[98]
	Caching Content	[109]	
	Optimal Position	[108]	[99]
	Optimal Position UE Association	[100]	
	Optimal Position UE Association UE Power Allocation		[101], [102]
	Optimal Position UE Association Bandwidth Allocation		[103], [104]
	Optimal Position UE Association UE Power Allocation Bandwidth Allocation		[105]–[107]

Fig. 7. Taxonomy for mobile IAB: types of mobility and studied topics.

February 19–23, 2018 in Japan. Two 5G eNBs were deployed operating at center frequency of 27.875 GHz, bandwidth of 700 MHz, and 2 antenna units each, with 96 antenna elements in each unit. Concerning the mobile equipment, it was mounted inside the train car, on the front windshield in front of the driver's seat with 64 antenna elements. The network was split into two sub-networks: an inter-server network between a master server at the BS and a cache server inside the train, and an end-user network between the cache server and the UEs inside the train. The UEs were downloading multiple 4K/8K video files. A maximum throughput of 2.08 Gbps was verified when the train was moving at a speed of 90 km/h.

In [68], the authors deployed an experimental setup for a proof-of-concept. In order to implement a handover-free communication of up to several tens of kilometers, they installed remote antenna units (RAUs) along the railway track and connected them to a central station. The RAUs were responsible for providing a wireless backhaul to a mobile BS installed on a train. The backhaul was deployed at W-band (75–100 GHz). UEs on the train communicated with the BS inside the train. They assumed that the train information, including location, velocity, and list of identified BSs, was available at the train operation center. This information was utilized to control and switch radio cells instead of using control signals as in cellular networks. They exploited transmission diversity with the Alamouti coding scheme and cell coordination between adjacent cells for interference cancellation. They successfully transmitted approximately 20 Gbps and 10 Gbps in downlink (DL) and UL, respectively.

Since the trains' internal network is almost considered as an independent network, state-of-the-art works usually focus on the backhaul link between the train antenna and external BSs, as is the case in [69], [70], [74]. More specifically, in [69], the authors investigated the power allocation problem between BSs and MRNs deployed on trains with the objective of maximizing system achievable sum rate. The proposed power allocation algorithm was based on multi-agent deep recurrent deterministic policy gradient (MADRDPG), which is capable of learning power decisions from past experience instead from an accurate mathematical model. Two constraints were considered. First, the power allocated to each MRN should not only be non-negative, but also be no more than the maximum transmitting power. Second, the minimum QoS requirements of each MRN should be met. They modeled the MADRDPG as: the state was represented by the MRNs channel gain of current time step, beamforming design of the current time step, and achievable rate and emitting power of the last time step; the action indicated the power allocated to each MR; and the reward was equal to the system achievable sum rate when the MRNs QoS constraints were satisfied, otherwise, it was zero. Simulation results showed that the proposed solution outperformed other state-of-the-art solutions based on machine learning.

As in [69], the authors of [70] also investigated the power allocation but focused on HO performance of HSR with MRN. This work also adopted the two-hop communication architecture, where the train passengers were served through MRNs. With such a two-hop transmission architecture, all

passengers within the train were treated as a "big user" of the BS. This avoided multiple simultaneously HO requests. Another addressed challenge related to HO was the impact of fading on HOs. Aiming at making the signal from different BSs more distinguishable, which results in better HO performance, the authors adjusted the power in the BSs' overlapping region by one parameter without knowing the precise CSI. More precisely, the overlapping region was divided into two sub-regions, one closer to the serving base station (sBS) and other closer to the target base station (tBS). Within the first subregion, the authors proposed to increase the transmit power of the sBS and decrease the transmit power of the tBS, while, within the second subregion, they proposed the opposite, i.e., increase the transmit power of the tBS and decrease the transmit power of the sBS. For this, they assumed perfect knowledge of trains' position. Mathematical analysis and simulation results showed that the proposed solution decreased the HO failure occurrence probability.

Finally, in [74], the authors investigated efficient hybrid beamforming (HBF) design for train-to-ground communications in mmWave. They developed a two-stage HBF algorithm in blockage-free scenarios. In the first stage, the MMSE method was adopted for optimal HBF design with low complexity and fast convergence. In the second stage, the orthogonal matching pursuit method was utilized to approximately recover the analog and digital beamformers. Furthermore, in blocked scenarios, they designed an anti-blockage scheme by adaptively invoking the proposed HBF algorithm, which can deal with random blockages. Simulation results showed that the proposed solution outperformed state-of-the-art solutions in terms of sum rate for different speed values and blockage probability.

A.2 Vehicular

Regarding mIAB deployed in vehicles, before presenting works that addressed system level problems, e.g., resource allocation and interference management, we present a more fundamental article that proposed a way to deploy a set of antennas in a vehicle to allow transmissions with good signal quality to and from mobile nodes.

The authors of [75] proposed an MRN setup configured with two groups of antennas on the roof of a vehicle: 1) the front predictor antennas; and 2) the behind receive antennas. In this way, the CSI acquired by front predictor antennas is exploited for data transmission to the behind receive antennas when they reach the same position, and the channel aging effect is minimized. If the receive antennas end up in the same position, it will experience the same radio environment, and the CSI will be almost perfect. If the receive antennas do not reach the same point as the predictor ones, due to, e.g., the processing delay is not equal to the time needed until the receive antennas reach the same point as the predictor ones, the receive antennas may receive the data in a place different from the one where the predictor antennas sent the pilots. Such spatial mismatch may lead to CSI inaccuracy, which deteriorates the system performance. Different methods based on transmission delay adaptation or rate adaptation are proposed to reduce the effect of spatial mismatch.

Similar to [75], other works from the literature have also already investigated the topic of predictor antennas from a theoretical perspective, e.g., [76], [77], and as experimental testbeds, e.g., [78].

The authors of [79], [80] analyzed the end-to-end outage probability and capacity at a vehicular UE of single-hop direct transmission (baseline case), and dual-hop transmission via an MRN as well as a fixed relay node. They assumed that the downlinks of different cells were synchronized in time, where the backhaul links were only active in the first time slot and access links were only active in the following slot. Thus, backhaul links and access links did not interfere with each other. By theoretical analyses and computational simulations the authors showed that in the cases of moderate to high vehicle penetration loss, MRNs deployed on top of vehicles enhanced QoS of the vehicular UEs compared to the scenarios with only direct transmission and with fixed relay nodes.

In [81], the authors of [79], [80] extended their study and compared the required average transmit power in similar scenarios under an outage probability constraint. They showed that dual-hop transmission via an MRN can also significantly reduce the power consumption of the network.

As the authors of [81], the authors of [82] also addressed the topic of energy efficiency. They proposed a Q-learning-based scheme to stabilize the energy efficiency of IAB nodes backhaul. For this, each mIAB node, i.e., vehicle-mounted APs, periodically reported its location and velocity to an access controller. The access controller was responsible for predicting the most suitable BS or device-to-device (D2D) node to serve the IAB nodes in the future and for configuring them to be connected to the predicted BS or D2D node. The IAB nodes, in their turn, were responsible for selecting a suitable transmission beamwidth and transmission power that kept the energy efficiency above a given threshold. The selection was performed by using a Q-learning based solution.

The resource allocation for macrocell UEs and the backhaul of the existing and newly arrived moving small cells deployed in vehicles was studied in [83]. The authors formulated the problem of maximizing the downlink data rate of the newly arrived moving small cells in the macrocell such that the data rate of the macrocell UEs and existing moving small cells UEs is protected. They proposed an adjustable-power-based resource allocation to allocate RBs and power in the macrocell.

The problem of resource sharing between moving cells and access links was also studied in [84]. More precisely, they considered a typical mobile cell scenario was considered, where in-vehicle cellular UEs are served by an in-vehicle antenna over the access link. A separate external antenna connects the mobile cells to the nearest eNB over the backhaul link, and to the neighboring mobile cells over the sidehaul link. The authors proposed algorithms to enable resource sharing between a mobile-cell, access link, sidehaul link and conventional cellular users taking into account interference caused by the wireless backhaul of mobile cells. The algorithms' performance was compared with the optimal, yet time-consuming, brute-force method and presented good results based on Monte-Carlo simulations.

The work [84] was extended in [85]. The authors proposed

new resource sharing and user scheduling algorithms that jointly aimed at ensuring that the access link shared the sub-channel either with backhaul link or with the out-of-vehicles macrocell UEs. They took into account results from [86] and [87], such as the minimization of interference to backhaul link and provisioning of high QoS for in-vehicle users by considering the use of directional access link antenna even at low transmit power. The authors also exploited the vehicular penetration loss along with self-interference-coordination to further reduce interference between the resource sharing links. They pointed as interesting direction for future research the deployment of the backhaul link for mobile cells through UAVs.

The problem of mutual interference between macro and moving small cell UEs is highlighted in [88]. Its authors studied the impact of deploying moving small cells in a Manhattan grid scenario in the presence of stationary traffic hotspot inside a macro cell. Simulation results showed that deploying moving small cells to offload traffic in the congested macro cell can be beneficial. However, when the small cells were moving far away from the traffic hotspot, the system performance was degraded compared to a network composed of only macro cells due to the high mutual interference between macro and small cell users.

A.3 Bus

In the context of mIAB considering buses, the majority of the works available in the literature focus on how to allocate resources in order to avoid the interference between access link of inside and outside UEs. A common adopted strategy is to split UEs into inside and outside UEs and allocate them in different parts of the spectrum. Another topic also addressed in the literature is related to HO from two perspectives: how to avoid multiple HO due to the mobility of the UEs and how to optimize the HO process considering that multiple UEs might change its sBS at the same time since they are moving together. In the following, we briefly discuss some papers.

The authors of [89]–[91] considered a macrocell with several public vehicles embedded with mobile femtocell access points (MFAPs). They proposed to deploy mmWave communications at 60 GHz inside vehicles for access links while the backhaul link of MFAPs and the direct link between an external UE and the macro cell use LTE. The authors analyzed three critical cases: a) the bus was near the eNB; b) two buses were close together; and c) an outside UE was close to a bus. They verified that, in case a), the eNB was a big interferer for inside UEs, because its transmission power was higher than that of the MFAPs. UEs served by the MFAPs measured a low SINR, and were forced to disconnect from MFAPs and connect to the eNB. This resulted in a high number of simultaneous HOs. However, as the bus moved, as soon as the signal of the MFAPs was acceptable, UEs had to re-engage to the MFAPs. In the case c), they showed that an outside UE in the proximity of a bus, especially when it was away from the sBS, could connect to the MFAPs, but its connection only lasted for a few minutes, depending on the speed of the bus.

Similar to [89]–[91], the authors of [92] considered moving femtocell deployed inside buses. The authors proposed a dynamic frequency allocation scheme that allocates the same frequency band for inside UEs even if they are in different buses, while the outside UEs are allocated in a different frequency band.

In [93], the authors also considered small cells deployed on the buses to serve the passengers. They studied the interference between moving small cells and proposed a probabilistic graph based resource allocation (PGRA) algorithm considering that the path of the moving small cell is fixed but it moves at non-uniform speed.

Different of [89]–[93], [86] proposed a model to allow the downlink backhaul sub-channels to be shared by in-vehicle downlink access link. This model is based on vehicular penetration effect and LOS communication. While vehicular penetration depends upon the material and construction properties of the transport vehicle, the LOS communication can be enabled using directional antennas. This paper also advocated that construction parameters and antenna positioning inside vehicles should be considered for future transport vehicles to increase the spectral efficiency for cellular network.

The authors of [86], extended their study in [87]. They presented new results regarding the exploitation of vehicular penetration effect and LOS communication to allow the downlink backhaul sub-channels to be shared by in-vehicle downlink access link transmission. Furthermore, a technique for access link power control was also proposed to reduce the interference to the backhaul link, while maintaining high link quality for in-vehicle users.

Regarding HO aspects of mIAB, the authors of [94] addressed the problem of group HO of UEs inside buses or trains. They proposed a resource management scheme that contains bandwidth adaptation policy and dynamic bandwidth reservation policy. More specifically, some instants before the moment when a bus or train is expected to arrive at a station, a given amount of resources at the station are reserved for the coming UEs. These resources remain reserved for a predefined interval of time. Simulation results showed that the HO call dropping probability considerably reduced compared to the case where no pre-reservation was performed without much impacting the bandwidth utilization.

The works [95], [96] also investigated the topic of HO in the context of mIAB. The authors of [95] analyzed the system performance of three different scenarios: in the first, there were only macro cells, in the second one there were macro cells and fixed femtocells and in the third one there were macro cells and mobile femtocells deployed in buses. The LTE technology was used for all links. The QoS of cell edge UEs improved after adding fixed and mobile femtocells. However, mobile UEs enjoyed better performance after adding the mobile femtocells, since these cells could reach areas that fixed femtocells could not. A result comparing the number of HOs considering three different HO strategies (namely, proactive, normal and reactive) was presented. In the presented results, the reactive strategy presented a lower number of HOs

compared to the other strategies. However, it was not presented how other metrics were impacted by these three strategies, e.g., link failure rate and UE throughput.

In [96], the authors considered a scenario with MRNs deployed at the top of buses and serving onboard UEs. They provided an analysis of the HO performance and the associated power consumption in LTE. Through computational simulations, the authors compared two cases. The first case was without MRNs deployed on the buses, meaning that all onboard UEs performed their individual HO procedure with macro eNBs. The second case was with MRNs, meaning that only the relays performed the HO procedure to the macro eNBs. Their results showed that the deployment of MRNs reduced the HO rate, the HO failure rate, the ping-pong rate, the UE power consumption and eNB power consumption. Furthermore, the simulation results also showed that UL transmission errors were the most dominant cause of MRNs HO failure. They highlighted that when deploying the relays, the HO procedure played an even more important role in keeping UEs connectivity. With the relays there was a single point of failure, i.e., when the relay HO failed, all UEs connected to the relay were dropped.

A.4 UAV

UAV-based MRN will not be part of the 3GPP Release 18 discussions on mIAB, and it is left for future uses in beyond 5G. However, it is still interesting to study its performance from an academic point of view. Compared to the previous types of mobility, e.g., trains and buses, UAVs have important differences. Firstly, in, e.g., buses, the MT and DU are installed outside and inside the buses, respectively, which gives good separation between them, while in UAVs this cannot be accomplished. Besides, UAVs are usually used to serve outside UEs so, for instance, the access links are also moving, but for buses the main purpose is to serve onboard UEs with stationary access links. More precisely, the main use-case for UAVs is coverage extension while for buses is capacity increment. Furthermore, a key point of UAVs is the chance for playing with their height while taking into account their energy consumption and lifetime, which are the main bottleneck for prolonged use of UAVs.

The integration of drones into cellular networks was addressed in [97]. Two different perspectives were presented: 1) how wireless networks can support personal or professional use of drones (called mobile-enabled drones (MEDs)); and 2) how drones can support wireless network performance, i.e., boosting capacity on demand, increasing, coverage range, enhancing reliability and agility as an aerial node called wireless infrastructure drones (WIDs). Regarding WIDs, different possibilities were addressed. One of them was the use of drones as IAB nodes. According to the authors, WIDs as intermediate IAB-nodes can reduce the number of hops, and provide topology flexibility thanks to LOS and mobility. More specifically, WIDs' mobility enables flexibility in topology design and alleviates the problem of coverage holes by following the crowd at the cell edge. They highlighted that co-channel interference may be a limiting factor.

Other advantages of the integration of UAVs were presented in [98]. They considered a scenario where UEs could connect to UAVs operating in mmWave, which co-existed with 5G NR BSs. Through mathematical analyses, they demonstrated that under certain speed, intensity, and service capacity, the use of UAV-based relays enabled significant gains for the system performance. In particular, outage probability and outage duration in the considered scenario became notably reduced, while spectral efficiency increased substantially.

The optimization of the UAV 3D-position in order to improve coverage is one of the most recurrent problems in the literature related to the deployment of UAVs as relay-nodes. The authors of [99] considered a ray tracing software called WinProp to study coverage of UAV-IAB nodes operating at mmWave. They considered two modes: amplify and forward (AF) and decode and forward (DF). Out-of-band and in-band IAB was assumed for AF and DF, respectively. For the AF case, the authors defined the power allocation based on the received backhaul link SINR. The UAVs were positioned so as to maximize the coverage. In the DF relaying mode, if the received SINR was above a certain threshold, a UAV forwarded its received packet. Trivial results were presented: UAVs improved coverage in the system compared with the case of IAB-donor only.

In [100], besides the optimal UAV positioning, the optimal UE-UAV association was also investigated. Their objective was to maximize the number of UEs served by the UAVs. The formulated problem was subject to a limited peak aggregate rate supported by the wireless backhaul link, a limited bandwidth available for access between UEs and UAV and a UE QoS requirement in terms of maximum path loss that a UE could tolerate before outage. Besides, the UEs could have different priorities to be served by the UAVs. The authors proposed a centralized solution, where for each candidate coordinate of the UAV-BS placement, the problem was transformed into a binary integer linear program, which was then solved through the branch-and-bound method.

In [101], the authors went even further. In order to maximize the overall instantaneous sum-rate, they tried to optimize 3D locations of the UAVs, UE-UAV/gNB association, UE-power allocation and precoder design at backhaul links. The authors considered a heterogeneous scenario with a macro BS and UAVs. DL was assumed. GNB had multiple antennas (massive MIMO) and UAVs had one receiving antenna and multiple transmit antennas. Terrestrial and aerial UEs had only one antenna. Aerial UEs received interference from DL signals to other aerial users, from gNB to terrestrial UEs, and from backhaul links (gNB to UAVs). UAVs are assumed FD. The following simplifying assumptions were made: ZF canceled out the intra tier interference (perfect CSI) and self-interference was completely eliminated at UAVs. The studied optimization problem was the maximization of the sum rate (instantaneous) at aerial and terrestrial UEs subject to SINR constraints and total available power at nodes. One of the main conclusions of the article was that the performance gains of using UAVs was increased when UEs were distributed in multiple hotspots far from each other in contrast to the case where UEs were in a single hotspot.

In [102], the authors of [101] extended their work. They proposed an interference management algorithm based on particle swarm optimization (PSO) to jointly optimize UE-UAV/BS association, downlink power allocations and the 3D deployment of UAVs in in-band UAV-assisted IAB networks. The UAVs were FD-capable. Two UAVs spatial configurations were compared. In the first one, the UAVs were configured as a single drone antenna array (DAA) to jointly serve ground UEs that were spatially distributed in a single hotspot. In that configuration, the UAVs did not interfere with each other. In the second configuration, the UAVs served the UEs in an independent way. The numerical results showed that, on one hand, when the ground cellular UEs were normally distributed into multiple bad coverage areas, the spatial configuration of distributed UAVs outperformed that of the DAA in terms of the overall network sum rate. On the other hand, when the ground cellular UEs were concentrated in a single bad coverage area, the spatial configuration of the DAA outperformed that of distributed UAVs. Numerical results confirmed that UAVs can be used for coverage improvement and capacity boosting in the IAB cellular networks.

In [103], besides of UAV placement and UE-UAV association, the authors also investigated resource allocation in an in-band IAB scenario. Orthogonal allocation was considered to avoid interference. Besides, in order to mitigate interference between macro-BSs and UAVs, reverse TDD between them is adopted, e.g., while the macro-BSs are in the DL mode with respect to their serving UEs, UAVs are in UL mode. The number of UL and DL slots are the same. HD is assumed at UAVs. UAVs can be seen as macro UEs. From the ground UEs' point of view, only interference from other UAVs is modeled. More specifically, the authors formulated an optimization problem to maximize the UE utility (log of data rate) subject to fronthaul and backhaul resources and user assignment. The problem was complex and a suboptimal approach was adopted. First, it was assumed fixed UAV placement and UE association and then the resource allocation was optimally solved. After that, user association and UAV placement were solved. Results showed the advantage of UAVs in heterogeneous networks (HetNets) and the relevance of the joint optimization considering fronthaul and backhaul constraints.

The problem of optimal UAV 3D positioning, UE-UAV association and resource allocation was also investigated in [104]. A scenario with one macro BS and multiple drone mounted base stations (DBSs) with in-band wireless backhaul was considered. As in [103], to reduce interference, reverse TDD was employed and access and backhaul links used orthogonal frequency channels. Besides, as the transmit power of DBS UEs was lower than that of a macro BS, the interference from the DBS UEs at macro BS UEs was assumed negligible. It was assumed that ultra-reliable low-latency communications (URLLC) UEs could only be connected to the macro BS in order to decrease latency, while enhanced mobile broadband (eMBB) UEs could be either associated directly to the macro BS or to a DBS. The formulated problem was decomposed into two sub-problems and solved as: 1) UE-BS association and wireless backhaul bandwidth

allocation were found through a primal decomposition method; and 2) the locations of DBSs were updated using the PSO algorithm. The authors concluded that clustered UEs could be covered with DBSs at lower altitudes, which can increase SNR. Furthermore, they also concluded that it was necessary to develop efficient interference cancellation methods for dense deployments of DBSs, since preventing overlapped areas among DBSs prevented DBSs to be deployed in its optimal locations.

In [105]–[107] the authors added another dimension to the list of optimized parameters of [104]. They also optimized the UE power allocation in addition to UAV 3D positioning, UE-UAV/BS association and resource allocation. In [105]–[107] the DBSs had in-band FD capabilities, while the UEs were HD capable. The focus was on DL. However, while in [105], the objective was to minimize the number of DBSs while maximizing the overall transmission rate, in [106], [107], the objective was only to maximize the total system throughput. The UEs could be either associated directly to a macro BS or to a DBSs. Neither different UEs nor different DBSs were scheduled at the same resources. However, it was assumed that DBSs could cancel part of their self-interference and due to this the backhaul link of a DBS reused the frequency spectrum of its access link. Due to the complexity of the problem (NP-hard), it was decomposed into two sub-problems: 1) DBSs placement problem (vertical and horizontal positions); and 2) Joint UE-BS association, power and bandwidth assignment problem. Approximation algorithms were proposed to solve the sub-problems. In [106], simulation results demonstrated gains of deploying DBSs compared to a system without them. In [107], the authors identified, for the considered scenario, a DBS altitude for which DBS position lower than that the path loss was dominated by the NLOS component, and DBS position higher than that the path loss was dominated by the LOS component.

Different of the previously mentioned works, [108] considered UL performance and a constraint on the UAV buffer. The authors of [108] also provided a short review of 3GPP technical reports (TRs) and decisions about UAV and IAB. They listed attractive UAV applications for mobile operators, e.g., wireless connection in disaster-affected regions, and network densification during temporary mass events. PSO was used to optimize UAV positioning. The authors concluded that as the number of UAV-nodes increased, the performance difference between static grid deployment of UAVs and dynamic positioning decreased, since a grid based deployment densely spanned across the entire service area, and all of the UEs were always within coverage of at least one UAV-BS. However, they highlighted that with an extremely high number of UAV-BS, the interference started to play an important role for the achievable throughput by not allowing the algorithm to position the UAV-BS as close as needed. Furthermore, they also showed that ideal backhaul scheme significantly overestimates the actual throughput, since all of the traffic generated by the UEs in the UAV-BS coverage area is usually assumed to be delivered to the APs successfully.

Besides the applications listed in [108], another use of UAVs was presented in [109]. In that paper, UAVs and ground small

cells were deployed to cache³ content close to the UEs in order to reduce traffic congestion in backhaul. UE association probability for the UAVs and the ground small-cells was derived using stochastic geometry. Besides, the successful content delivery probability was also derived by considering both the intercell and intracell interference. The successful content delivery performance has been improved by 26.6% on average by caching popular content in the UAVs.

V. PERFORMANCE EVALUATION

This section presents a performance comparison between a scenario with mIAB and two benchmark scenarios: one with only macro gNBs, called here as *only macros* scenario, and other with macro and pico gNBs fiber-connected to the CN, called here as *macros-picos* scenario. The details concerning the considered simulation modeling are presented in Section V-A and the results are discussed in Section V-B.

A. Simulation Assumptions

It was considered a simplified version of the Madrid grid [110] as in [111]. As illustrated in Fig. 8, in this scenario, there were nine square blocks, with dimension of $120\text{ m} \times 120\text{ m}$. The blocks were surrounded by 3 m wide sidewalks and separated of each other by 14 m wide streets with four lanes, two in each direction. In the central block there were 3 not co-located macro gNBs deployed as in Fig. 8. Pedestrians and buses were randomly placed in the sidewalks and in the streets, respectively. In the intersections, they had a probability of 60 % to continue straight ahead and 40 % to turn left or right with equal probability to each side. The pedestrians walked in the sidewalks and were allowed to cross the roads only in the intersections. Passengers were randomly located inside the buses at any available seat. During the simulation, their position relative to their bus did not change. In the mIAB scenario, mIAB nodes were deployed at the buses. The DU and MT were placed at the back of the buses; however, the DU was inside and the MT was outside at the roof. Important to mention that an mIAB node could not connect to another mIAB node. It could only be served by an IAB donor, i.e., a gNBs. Other parameters related to the entities present in the system, e.g., IAB donors, mIAB nodes, pedestrians and passengers, are presented in Table I.

The simulations were conducted at 28 GHz with 50 MHz of system bandwidth. The channel link between the entities present in the simulations was modeled using the 5G-SToRM channel model described in [113], where [113] implements its channel model according to [112]. The adopted channel model from [112], [113] is spatially and time consistent. It considers a distance-dependent path-loss, a lognormal shadowing component and a small-scale fading. Moreover, as illustrated in Fig. 9, all the links with the donor, i.e., donor-pedestrian, donor-MT, donor-DU and donor-passenger, were modeled as urban macro (UMa). All links involving the MT, except the link donor-MT, were modeled as urban micro (UMi), as well as the links DU-pedestrian and pedestrian-passenger.

³The use of cache has not been standardized in 3GPP.

TABLE I
ENTITIES CHARACTERISTICS.

Parameter	IAB Donor	mIAB node - DU	mIAB node - MT	Pedestrian	Passenger
Height	25 m	2.5 m	3.5 m	1.5 m	1.8 m
Transmit power	35 dBm	24 dBm	24 dBm	24 dBm	24 dBm
Antenna tilt	12°	4°	0°	0°	0°
Antenna array	URA 8 × 8	URA 8 × 8	ULA 64	Single antenna	Single antenna
Antenna element pattern	3GPP 3D [112]	3GPP 3D [112]	Omni	Omni	Omni
Max. antenna element gain	8 dBi	8 dBi	0 dBi	0 dBi	0 dBi
Speed	0 km/h	40 km/h	40 km/h	3 km/h	40 km/h

TABLE II
TDD SCHEME ADOPTED IN ONLY MACROS AND MACROS-PICOS SCENARIOS.

Slot	1	2	3	4	5	6	7	8	9	10	DL usage	UL usage	Total usage
Macro and Pico gNBs	DL	S (DL)	UL	UL	UL	DL	S (DL)	UL	UL	DL	50%	50%	100%

TABLE III
TDD SCHEME ADOPTED IN THE MIAB SCENARIO.

Slot	1	2	3	4	5	6	7	8	9	10	DL usage	UL usage	Total usage
IAB donor	DL	UL	∅	DL	∅	UL	DL	∅	UL	DL	40%	30%	70%
Backhaul	DL	∅	UL	DL	UL	∅	∅	UL	∅	DL	30%	30%	60%
IAB node	∅	UL	DL	∅	DL	UL	DL	DL	UL	∅	40%	30%	70%

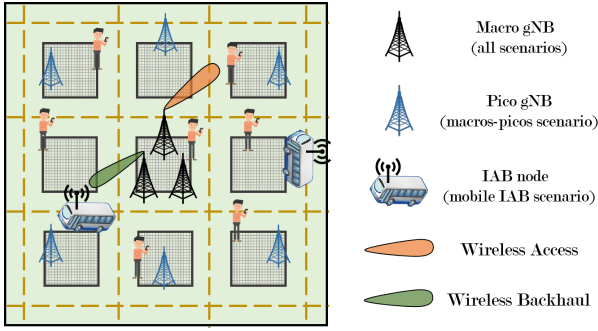


Fig. 8. Simplified Madrid grid.

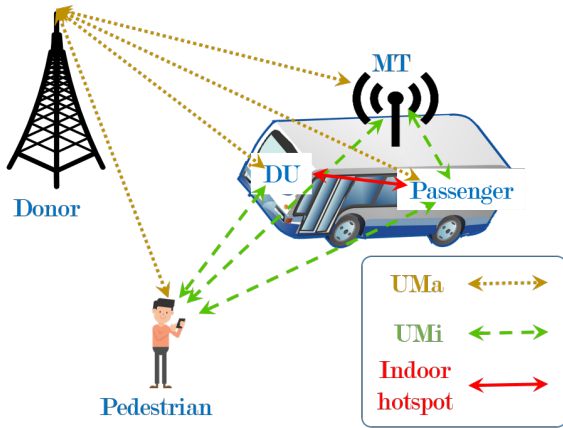


Fig. 9. Channel types.

The link DU-passenger was modeled as an indoor hotspot one. The bus body had a penetration loss of 40.1 dB [91]. Thus, the links with one entity inside the bus and other outside, such as donor-DU, DU-pedestrian, MT-passenger

and pedestrian-passenger, suffered this penetration loss. Furthermore, the link between a DU of a bus and a passenger of another bus suffered twice this penetration loss. Besides, all the links that crossed the bus body were considered NLOS. The other links could be either in LOS or NLOS with a transitional state between them as described in [112].

Regarding resource scheduling, a slot was the minimum scheduling unit. In the time domain, a slot consisted of 14 orthogonal frequency division multiplexing (OFDM) symbols with total time duration of 0.25 ms, while in the frequency domain it consisted of one resource block (RB) with subcarrier spacing of 60 kHz, where one RB corresponded to 12 consecutive subcarriers.

In the frequency domain, the round robin (RR) scheduler was adopted to schedule the RBs. The RR iteratively allocated the RBs, scheduling in a given RB the UE bearer waiting the longest time in the queue. In the access links, multiple input single output (MISO) transmissions were performed with a matched filter used as precoder. On the other hand, in the backhaul, MIMO transmissions were performed. To take advantage of the multiple antennas at both sides of a backhaul link, the transmission within an RB was multiplexed into streams. For each stream, it was computed a pair of precoder/decoder using the singular value decomposition (SVD) of the channel between an IAB donor and the MT part of an mIAB node. At most the eight streams with the highest singular values were scheduled, subject to having an estimated modulation and coding scheme (MCS) higher than one.

In the time domain, TDD schemes were used to separate transmission and reception of the signals, i.e., in a given slot, data could traverse a link in just one direction, either UL or DL. More specifically, the TDD scheme presented in Table II was considered in the only macros and macros-picos scenarios,

while the TDD scheme in Table III was considered in the IAB scenario, where backhaul UL means that the mIAB MT part transmits data to the IAB donor, while backhaul DL means that the mIAB MT part receives data from the IAB donor. The TDD scheme in Table II is standardized by 3GPP in [114], while the one in Table III is based on the one proposed in [26] for three hops (in our case we are considering just two hops). Remark that on the one hand, in the scheme of Table II, macro and pico gNBs are active in 100% of the time, transmitting either in DL or in UL with equal time usage for both DL and UL. On the other hand, in the scheme of Table III, IAB donor and mIAB node are active only in 70% of the time and with different time usage between DL and UL. One of the reasons for this is the introduction of silence intervals to reduce interference in the system. Specifically regarding the buses, to avoid self-interference, they could not simultaneously receive and transmit data, e.g., receive in the MT while transmitting in the DU.

As a measure of signal strength, the UEs and the mIAB nodes were measuring the reference signal received power (RSRP) of candidate serving cells, where the RSRP is the linear average over the power contributions (in Watts) of the resource elements confined within a SSB transmitted by a candidate serving cell, as defined in [115]. The topology adaptation was based on the highest measured RSRP. The channel quality indicator (CQI)/MCS mapping curves standardized in [116] were used for link adaptation with a target block error rate (BLER) of 10%. It was also considered an outer loop strategy to avoid the increasing of the BLER. According to this strategy, on the one hand, when a transmission error occurred, the estimated SINR used for the CQI/MCS mapping in the link adaptation was subtracted by a back-off value of 1 dB. On the other hand, when a transmission occurred without error, the estimated SINR had its value added by 0.1 dB.

As previously mentioned, three scenarios were considered. The first with only three macro gNBs deployed at the central block, called here as only macros scenario. The second with the three macro gNBs (acting as IAB donors) plus mIAB nodes deployed in the buses, called here as mIAB scenario. The third with the three macro gNBs plus 6 pico gNBs deployed at the positions indicated in Fig. 8 (at the vertices of a hexagon) called here as macros-picos scenario. In these three scenarios there were 6 buses (as many as pico gNBs) and 72 UEs, i.e., passengers plus pedestrians. The UEs' traffic, in both DL and UL, was modeled as constant bit rate (CBR) flows with packet-inter-arrival time equal to four slots. In the simulations, it was analyzed the impact of the packet size and the impact of the percentage of passengers considering the 72 UEs in the system. For this, nine possible combinations of packet size and percentage of passengers were tested, where the packet size could be equal to 1024, 2048 or 3072 bits and the percentage of passengers considering the 72 UEs in the system could be equal to 25%, 50% or 75% meaning that in each bus there were 3, 6 or 9 passengers. Table IV summarizes the main simulation parameters.

In the following, the simulation results are presented. Firstly, we compare the downlink performance of passengers

TABLE IV
SIMULATION PARAMETERS.

Parameter	Value
Layout	Simplified Madrid grid [110], [111]
Carrier frequency	28 GHz
System bandwidth	50 MHz
Subcarrier spacing	60 kHz
Number of subcarriers per RB	12
Number of RBs	66
Slot duration	0.25 ms
OFDM symbols per slot	14
Channel generation procedure	As described in [112, Fig.7.6.4-1]
Path loss	Eqs. in [112, Table 7.4.1-1]
Fast fading	As described in [112, Sec.7.5] and [112, Table 7.5-6]
AWGN power per subcarrier	-174 dBm
Noise figure	9 dB
Mobility model	Pedestrian and Vehicular [117]
Number of buses	6
Passengers + pedestrians	72
Percentage of passengers	{25%, 50%, 75%}
Number of passengers per bus	{3, 6, 9}
CBR packet size	{1024, 2048, 3072} bits
CBR packet inter-arrival time	4 slots

and pedestrians in the three considered scenarios, focusing on their throughput, latency and MCS usage. Secondly, we analyze their performance on the uplink, highlighting the main differences compared to the downlink. Then, we focus on the wireless backhaul quality in the mIAB scenario. Finally, we present the statistics of links served by the IAB donors. More specifically, we analyze the percentage of time that the IAB donors served backhaul and access links.

B. Simulation Results

B.1 Downlink

Downlink Throughput

Firstly, let's analyze the impact of introducing mIAB on the DL throughput of passengers and pedestrians. Figure 10 presents the DL throughput of passengers (dashed lines) and pedestrians (solid lines) considering a packet size of 3072 bits and for three different percentages of passengers.

First, notice that in the three figures of Fig. 10, the DL throughput of passengers in the mIAB scenario (blue dashed lines with circles as markers) was similar for almost 100% of them. This was due to their vicinity to the mIAB node, i.e., they were next to the DU antennas inside the buses. Besides, compared to the only macros scenario (green dashed lines with triangles as markers), in the mIAB scenario, the DL throughput of the majority of the passengers was remarkably improved. One could argue that in the mIAB scenario there were more gNBs, i.e., the ones in the buses, than in the only macros scenario. However, even when compared to the macros-picos scenario (orange dashed lines with squares as markers), where the number of gNBs was equal to the one in the mIAB scenario, the passenger DL throughput of mIAB scenario was higher than the one for macros-picos scenario in most of the

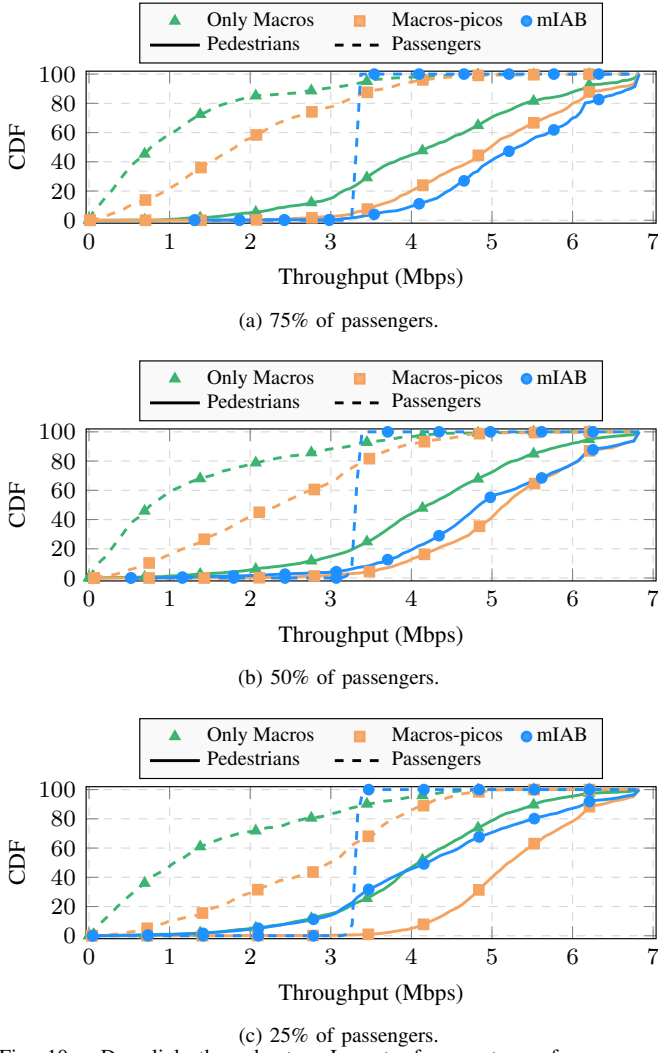


Fig. 10. Downlink throughput – Impact of percentage of passengers, considering packet size equal to 3072 bits.

percentiles. Besides, while the DL throughput of all passengers in the mIAB scenario was higher than 3 Mbps, more than half of the passengers in the macros-picos scenario were not able to achieve this throughput. The main reason for this is the fact that signals serving passengers in the only macros and macros-picos scenarios suffered a penetration loss of 40.1 dB, due to the signal crossing the bus body, while, in the mIAB scenario, the passengers were connected to antennas deployed inside the bus that did not suffer this loss.

Regarding the pedestrians DL throughput in the mIAB scenario, we can see in Fig. 10, that it varied with the percentage of passengers in the system, thus, with the number of pedestrians. Decreasing the percentage of passengers, i.e., increasing the number of pedestrians, their DL throughput decreased. One of the reasons was the adopted fixed IAB TDD scheme, Table III, which partitioned the slots between backhaul and UEs directly connected to IAB donors without taking into account the real necessity of the system. Thus, it could be better if one adopted a dynamic resource scheduling taking into account the load of backhaul and UEs directly connected to the IAB donors. Besides, compared to the other scenarios, in the IAB scenario, the IAB donors, which served

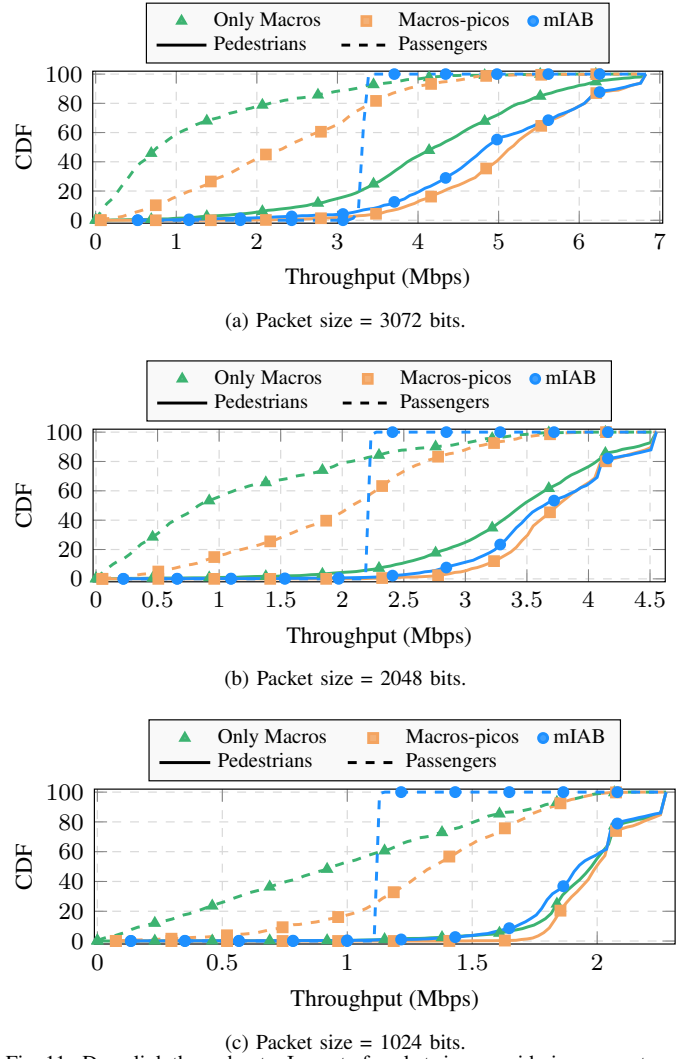


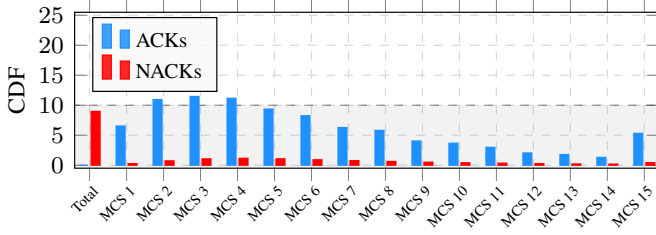
Fig. 11. Downlink throughput – Impact of packet size, considering percentage of passengers equal to 50%.

most part of the pedestrians, were active in the DL only in 40% of the time, while in the other scenarios, according to the adopted TDD scheme in Table II, the macro gNBs were active in the DL during 50% of the time. However, we remark that even if the pedestrians DL throughput decreased in the mIAB scenario compared to the others, it still achieved values high enough to keep a good connectivity.

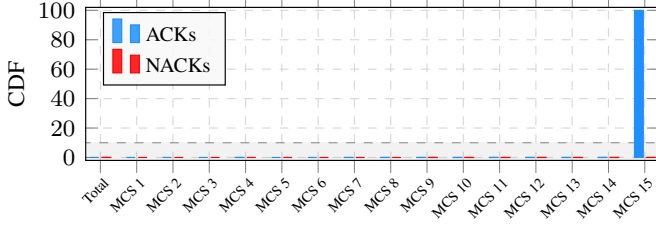
Figure 11 also presents the DL throughput of passengers (dashed lines) and pedestrians (solid lines), but for three different packet sizes and considering 50% of the UEs in the system as passengers. Similar to the analyses of Fig. 10, we can conclude here that the deployment of mIAB nodes inside the buses improved the passengers DL throughput, while keeping the pedestrians with a good DL throughput. Furthermore, we highlight that for higher percentages of passengers in the system and higher packet size, i.e., more loaded systems, the gains of using mIAB relative to the only macros and macros-picos scenarios were higher.

Downlink Data Transmission Quality

Figures 12a and 12b present the passengers' MCS usage in DL for the only macros and mIAB scenarios, respectively for



(a) Only macros scenario.



(b) mIAB scenario.

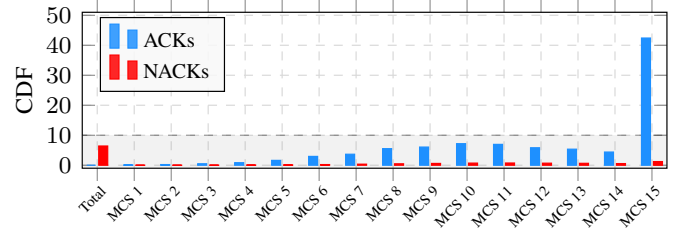
Fig. 12. Histogram of passengers' MCS usage in DL in a scenario with 50% of passengers and packet size of 3072 bits.

the configuration with 50% of passengers in the system and packet size of 3072 bits. The red bars represent the percentage of transmissions with error and the blue bars represent the percentage of successful transmissions. First, we remark that Fig. 12b does not refer to the passengers end-to-end link quality (IAB donor - passengers), it only refers to the quality of the link between the mIAB nodes and their served passengers. The quality of the link between the IAB donors and the mIAB nodes will be analyzed in Section V-B3.

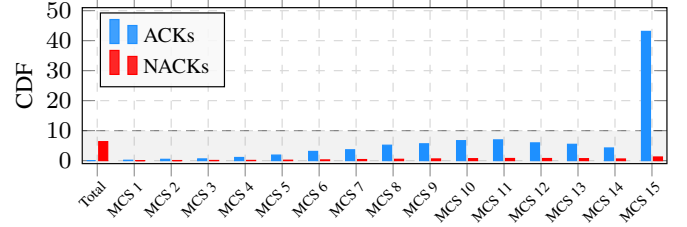
On the one hand, notice that in Fig. 12a, in the only macros scenario, the passengers received data mainly with lower MCSs. This was mainly due to the bus penetration loss, which degraded the link between passenger and macro gNBs. On the other hand, notice that in Fig. 12b, in the mIAB scenario, the passengers received data from the mIAB node with the highest MCS and with almost zero transmission error. This is a benefit of deploying the DU part of the mIAB node inside the buses.

The pedestrians' MCS usage in DL is presented in Fig. 13. Figure 13a is related to the only macros scenario, while Fig. 13b concerns pedestrians connected to an IAB donor in the mIAB scenario and Fig. 13c concerns pedestrians connected to an mIAB node also in the mIAB scenario. First, notice that the histograms in Fig. 13a and Fig. 13b are similar with small differences, meaning that the SINR of a pedestrian connected to a macro gNB in the only macros scenario and the SINR of a pedestrian connected to an IAB donor in the mIAB scenario were similar. Furthermore, considering that the pedestrian signal strength was also similar in both cases, since the macro gNB and the IAB donor had similar characteristics, we conclude that the interference in both cases was also similar.

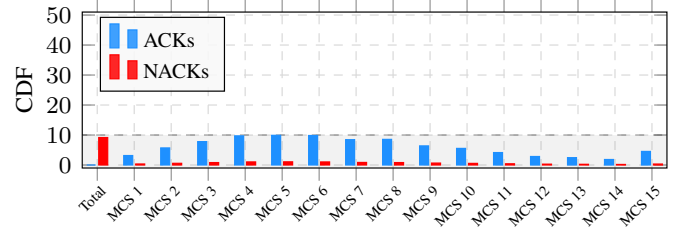
In the mIAB scenario, 15% of the pedestrians were served by an mIAB node for at least a couple of transmission time intervals (TTIs). Particularly, their connection lasted less than 1 s in 90% of the cases, as illustrated in Fig. 14, which



(a) Only macros scenario.



(b) mIAB scenario - pedestrians connected to an IAB donor.



(c) mIAB scenario - pedestrians connected to an mIAB node.

Fig. 13. Histogram of pedestrians' MCS usage in DL in a scenario with 50% of passengers and packet size of 3072 bits.

is not good in practice. They connected to a mIAB node due to a higher RSRP. However, when they were receiving data from the DU part of the mIAB node, the MT part was transmitting upstreaming data to the IAB donor in the backhaul, as described in Table III slots 3, 5 and 8. Thus, the MT part of the mIAB node caused a high interference to the pedestrians connected to an mIAB node, since both were active at the same time and both were outside the bus, meaning that the interfering link did not suffer attenuation due to the crossing of the bus body. This inference caused low values of SINR and so the usage of low MCSs as shown in Fig. 13c. Important to remark that this interference was not a problem for the passengers, since they were inside the bus and the signal from the MT part suffered from the bus body penetration loss.

Based on these results, one can conclude that pedestrians should avoid connecting to an mIAB node, unless the signal between them is strong enough to compensate the interference from the MT part and the connection is expected to last longer than a given threshold. For this, one could consider an admission policy to allow a UE to connect to a mIAB cell. The admission criteria could be: a minimum measured RSRP value; a maximum measured interference level (reference signal received quality (RSRQ) instead of RSRP); the relative UE and bus geographical position in a given time interval; etc..

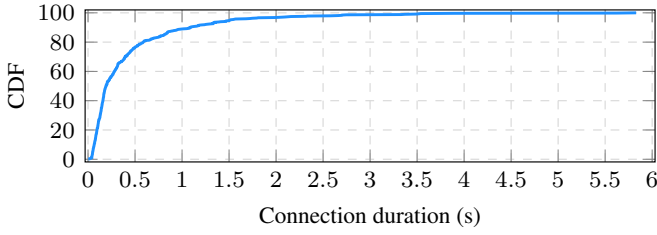
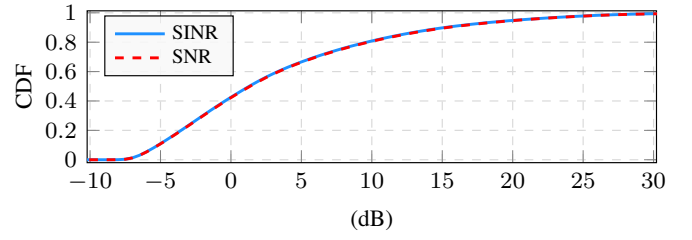
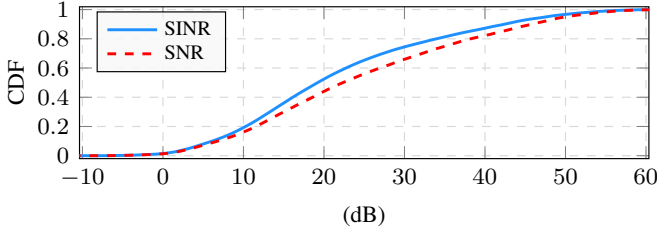


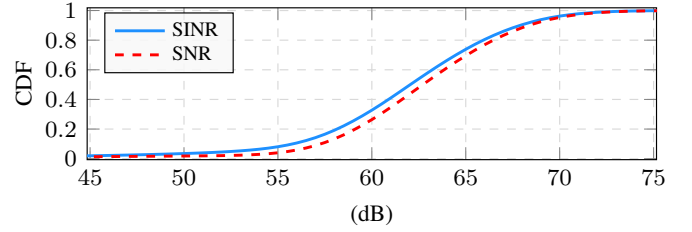
Fig. 14. CDF of connection duration between a pedestrian and a mIAB node.



(a) Only macros scenario.

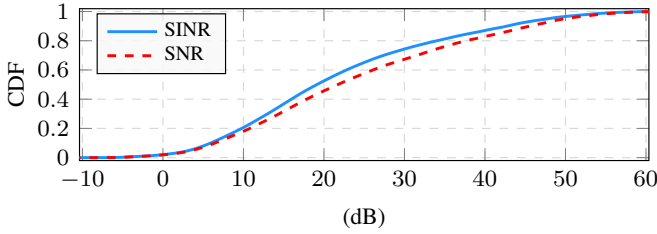


(a) Only macros scenario.



(b) mIAB scenario - passengers connected to a mIAB.

Fig. 16. SINR and SNR of passengers in a scenario with 50% of passengers and packet size of 3072 bits.



(b) mIAB scenario - pedestrians connected to an IAB donor.

Fig. 15. SINR and SNR of pedestrians in a scenario with 50% of passengers and packet size of 3072 bits.

Figures 15a and 15b present the CDF of SINR and SNR in the DL of pedestrians connected to a macro gNB in the only macros and mIAB scenarios, respectively. Comparing these two figures, notice that the difference between the SINR and SNR curves, i.e., the interference, is similar (the difference neither increased nor decreased when changing the scenario). Thus, we can conclude that the deployment of mIAB nodes may not impact the interference that the pedestrians connected to a macro gNB suffered. This is an important result, since the possible dynamic interference caused by mIAB nodes in the UEs served by IAB donors is one of the concerns regarding the deployment of mIAB cells. The interference avoidance was obtained due to the adopted TDD scheme (Table III), which did not allow transmissions in the access links of mIAB nodes when IAB donors were operating in DL in their access links. The topic of exploiting a TDD scheme for interference handling in mIAB networks is addressed in [118].

Figures 16a and 16b present the CDF of SINR and SNR in the DL of passengers connected to a macro gNB in the only macros scenario and connected to an mIAB node in the mIAB scenario, respectively. In Fig. 16a, the SINR and SNR curves are superposed, meaning that in the only macros scenario the interference was not a problem for the passengers. This was a consequence of the bus body loss that filtered possible interference links coming from neighbor gNBs. The drawback of the bus body loss is that it filters not only the

interference but also the signals serving the passengers, as we can see by the low values of the SNR. In this scenario, 80% the passengers had an SNR lower than 10 dB. On the other hand, in the mIAB scenario, their SNR had a boost when deploying the mIAB nodes in the buses (Fig. 16b). In this scenario, when the backhaul (MT part of the mIAB nodes) was operating in the UL, they interfered with the passengers receiving in the DL from the DU part of the mIAB nodes. However, as we can see in Fig. 16b, the SINR was still high enough to allow transmissions with the highest MCS.

Downlink Latency

DL transmissions with low MCS, thus low DL throughput, to the passengers in the only macros and macros-picos scenarios impacted the passengers DL latency as it can be seen in Fig. 17 and Fig. 18. These figures present the CDF of the UEs end-to-end DL latency for different values of the percentage of passengers and of the packet size, respectively. Dashed and solid curves represent the DL latency of passengers and pedestrians, respectively. On the one hand, one can see that passengers using delay sensitive services will suffer in the only macros and macros-picos scenarios, since in the simulations their DL latency achieved values up to 6 s. On the other hand, in the mIAB scenario, DL packet latency was negligible. In that scenario, for the majority of the passengers, in the worst case, the latency was equal to 2 ms. It corresponded to the case where packets were generated in the IAB donor at slot 5 of Table III and needed to wait until slot 10 to be transmitted in the backhaul from the IAB donor to the mIAB node and only at the next slot 3 of the next frame it was transmitted from the mIAB node to the passengers, totalizing 8 slots, i.e., 2 ms, of delay. Furthermore, similar to the analyses of DL throughput, we can see that for higher percentages of passengers in the system and higher packet size, i.e., more loaded systems, the gains in the mIAB scenario for

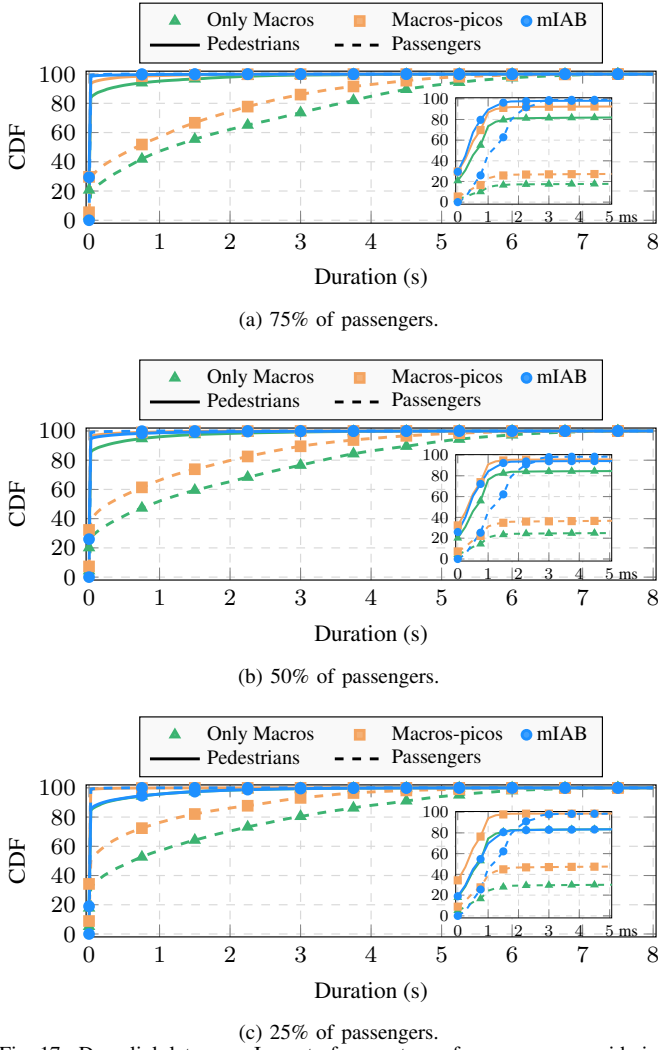


Fig. 17. Downlink latency – Impact of percentage of passengers, considering packet size equal to 3072 bits.

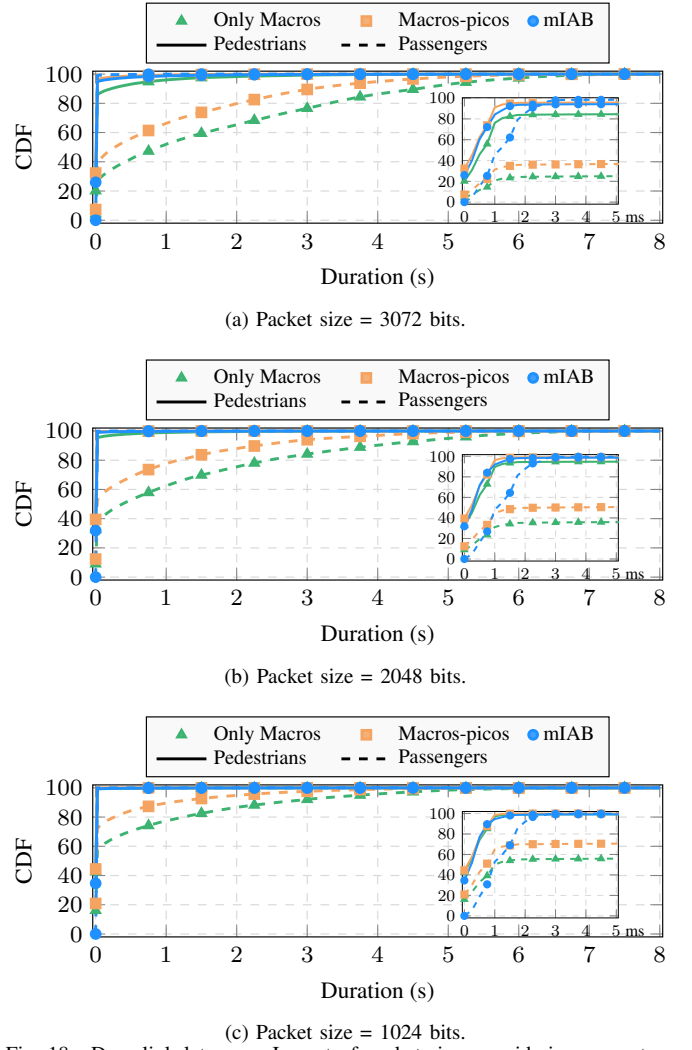


Fig. 18. Downlink latency – Impact of packet size, considering percentage of passengers equal to 50%.

the passengers DL latency were higher compared to the other scenarios.

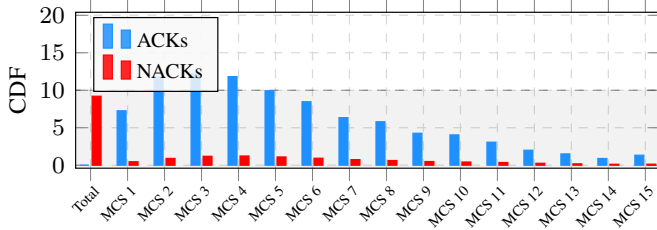
B.2 Uplink

Until now, we have analyzed the mIAB performance in the DL. Now, let's focus on the UL. In general, in the UL we came to similar conclusions as the ones drawn in the DL analyses. However, due to different transmit power and interference pattern in DL and UL, some points were different and will be highlighted in the following.

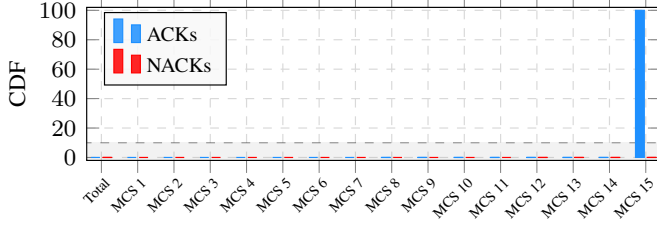
Figure 19 presents the passengers' MCS usage in UL for the only macros and the mIAB scenarios for the configuration with 50% of passengers in the system and packet size of 3072 bits. It is equivalent to Fig. 12, but for the UL. The red bars represent the percentage of transmissions with error and the blue bars represent the percentage of successful transmissions. Comparing Fig. 12a and Fig. 19a, one can notice that in the DL of the only macros scenario, even if the majority of the transmissions were with lower MCSs, 5% of the transmissions were successful with the highest MCS. However, in the UL, less than 1.5% of the transmissions were successful with the highest MCS. The main reason for this was the lower transmit

power in the UL compared to the DL. As a consequence, the SINR of the passengers was lower, allowing them to mostly use only the lowest MCSs.

The pedestrians' MCS usage in UL is presented in Fig. 20. Figure 20a is related to the only macros scenario, while Fig. 20b concerns pedestrians connected to an IAB donor in the mIAB scenario and Fig. 20c concerns pedestrians connected to an mIAB node also in the mIAB scenario. Figure 20 is equivalent to Fig. 13, but for the UL. Comparing Fig. 13c and Fig. 20c, one can notice that, for the pedestrians connected to an mIAB node, in the DL, only 5% of the transmissions were successful with the highest MCS, while, in the UL, 13% of the transmissions were successful with the highest MCS. This difference is explained by the fact that, even though the transmit power in the UL was lower, the interference was even lower. More precisely, analyzing Table III, we can see that a pedestrian connected to an mIAB node receiving data in the DL suffered interference from the MT part of the mIAB node, which was transmitting in the UL to the IAB donor and which did not suffer from the bus penetration loss since it was placed outside the bus. However, when the same pedestrian was transmitting in the

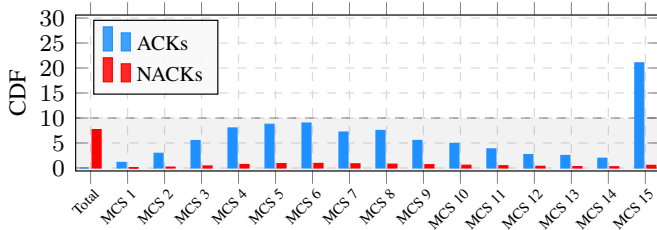


(a) Only macros scenario.

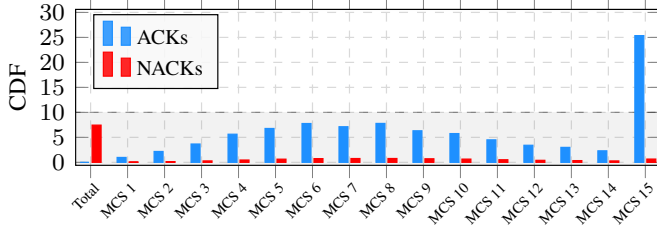


(b) mIAB scenario.

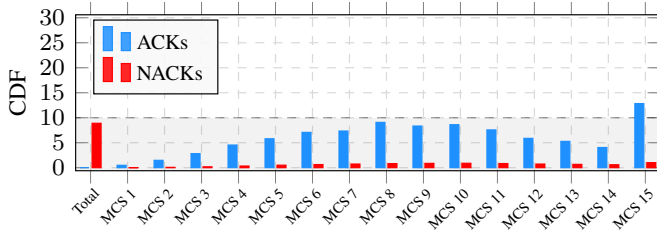
Fig. 19. Histogram of passengers' MCS usage in UL in a scenario with 50% of passengers and packet size of 3072 bits.



(a) Only macros scenario.



(b) mIAB scenario - pedestrians connected to an IAB donor.



(c) mIAB scenario - pedestrians connected to an mIAB node.

Fig. 20. Histogram of pedestrians' MCS usage in UL in a scenario with 50% of passengers and packet size of 3072 bits.

UL to the DU part of an mIAB node, the DU part suffered interference from other pedestrians connected to the IAB donor and transmitting data to it in the upstreaming. Thus, the interference that they caused in the DU also suffered from the bus penetration loss.

The highlighted differences regarding the MCS distribution

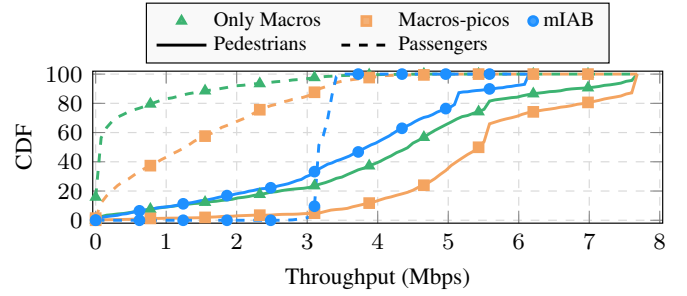


Fig. 21. Uplink throughput considering packet size equal to 3072 bits and percentage of passengers equal to 50%.

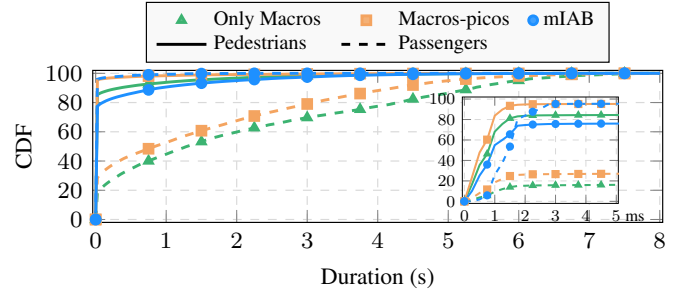


Fig. 22. Uplink latency considering packet size equal to 3072 bits and percentage of passengers equal to 50%.

impacted the UL throughput. Figure 21 presents the UL throughput of passengers (dashed lines) and pedestrians (solid lines) considering packet size equal to 3072 bits and percentage of passengers equal to 50%. It is equivalent to Fig. 10b, but for the UL. As we have seen, the link quality of passengers in the only macros scenario was worse in the UL than in the DL due to the lower transmit power. As a consequence, in the only macros scenario, passengers UL throughput was worse than their DL throughput, as one can see comparing Fig. 21 and Fig. 10b. Thus, for the passengers, the gains of deploying mIAB, in terms of throughput, were even higher in the UL. Concerning the pedestrians, in the mIAB scenario, their UL throughput was lower than their corresponding DL throughput. It is explained by the fact that, in the adopted TDD scheme for the mIAB scenario, less time slots are used for UL transmissions than for DL transmissions.

Figure 22 presents the UL latency results. It is equivalent to Fig. 17b, which presents the DL latency results. Conclusions similar to the ones obtained from the UL throughput can be drawn regarding the UL latency.

B.3 Backhaul Quality

In a mIAB scenario, besides the quality of the links of passengers and pedestrians, one should also be careful with the quality of the backhaul link, since when a bus suffered from a bad link to their serving IAB donor, all the passengers connected to it also suffered. Figure 23 presents the histogram of DL and UL backhaul's MCS usage in a scenario with 50% of passengers and packet size of 3072 bits. Comparing Fig. 23a and Fig. 23b with Fig. 12a and Fig. 19a, respectively, one can again conclude that it was better for a passenger to communicate with the IAB donor through an mIAB node

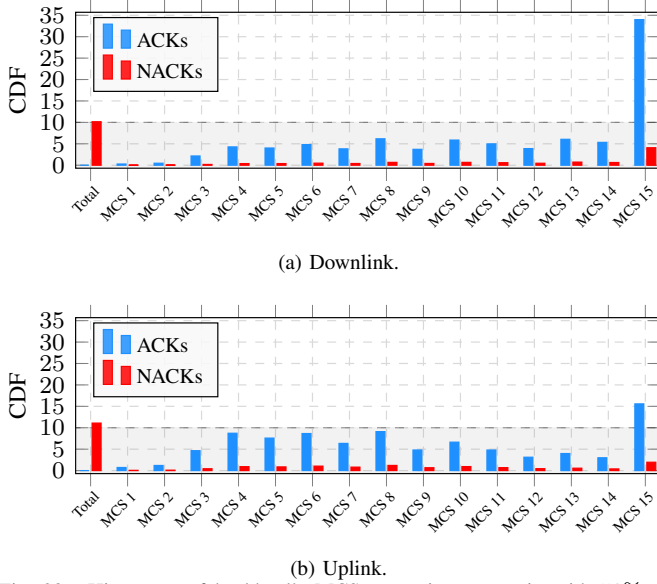


Fig. 23. Histogram of backhaul's MCS usage in a scenario with 50% of passengers and packet size of 3072 bits.

instead of being directly connected to it. The backhaul better link quality was mainly due to the deployment of the mIAB node MT part outside the bus, thus overcoming the bus penetration loss, and also due to the utilization of a uniform linear array (ULA) with 64 antenna elements instead of a single antenna as the passengers did.

B.4 Links Served by IAB Donors

We have seen that the adopted TDD scheme impacts the results. Thus, it is interesting to try to understand how to better allocate the resources. For this, it is important to understand the profile of the links served by the IAB donors. Hence, in this part we analyze the number of links served by the IAB donors, the percentage of them that are access links and how many links are served by the IAB donors in the backhaul of mIAB nodes.

Figure 24 presents the histogram of the number of links served by IAB donors. When serving a bus, i.e., an mIAB node, an IAB donor indirectly served through the backhaul the UEs served by the bus (almost always, only passengers). Thus, when a bus disconnected from the IAB donor, the load in the donor suddenly changed a lot, since the passengers went away together with the bus. Due to this, as we can see in Fig. 24 the number of links served by an IAB donor could be quite different from one donor to another, since if they served a different number of buses, the difference in the number of served links was approximately multiple of the number of passengers per bus.

This effect is well visible in Fig. 24a, which refers to the case of 75% of passengers in the system, i.e., nine passengers per bus. Notice that, in this figure, there are six peaks (six was the number of buses in the simulations), each one centered in a multiple of nine, which is the number of passengers in a bus for this case. When the number of passengers was reduced from nine to six and three as in Fig. 24b and Fig. 24c, respectively, the load variability of the IAB donors decreased,

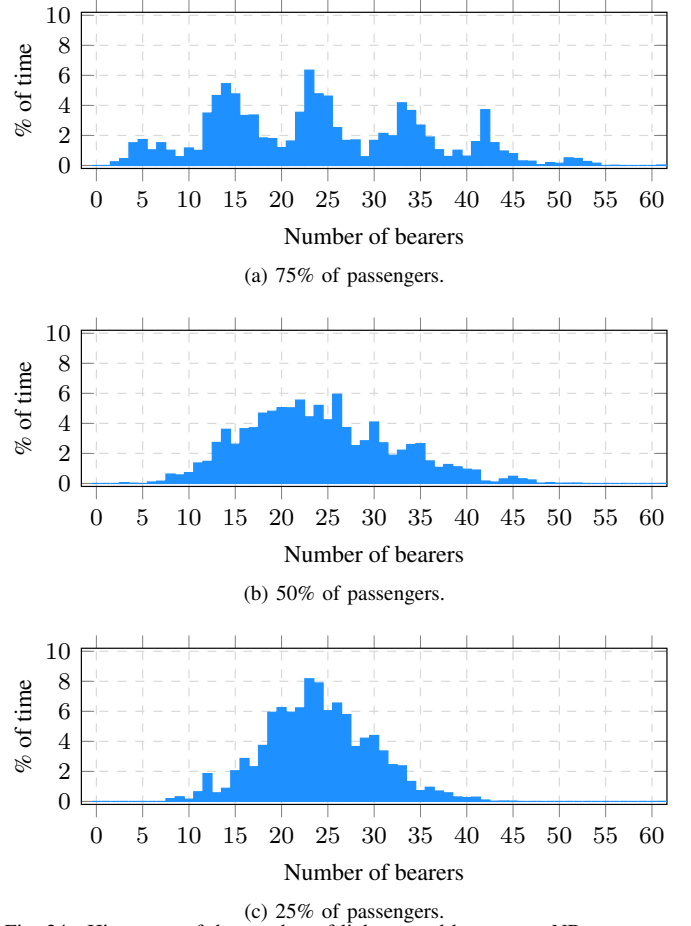


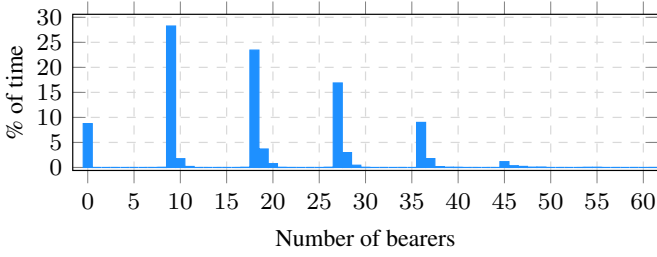
Fig. 24. Histogram of the number of links served by macro gNBs.

since, in those cases, moving a bus from one IAB donor to another did not heavily impact the load of those donors.

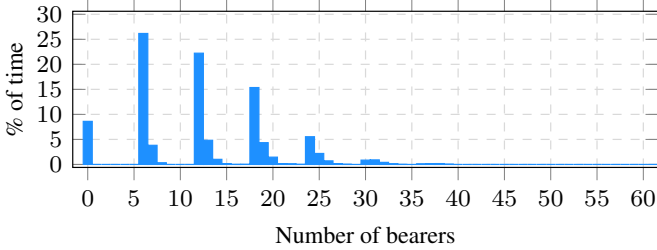
Based on these results, one should consider adopting topology adaptation strategies that take into account the IAB donor load. This may avoid overloading IAB donors when changing the serving donor of a given bus.

Figure 25 focuses only on the number of backhaul links served by IAB donors and presents the histogram of this number. Since, in the backhaul, the IAB donors were serving links from the buses, one could expect that through the backhaul the donors would serve a number of links multiple of the number of passengers in the buses. However, Fig. 25 shows that sometimes the backhaul served a number of links a little bit higher than a number multiple of the number of passengers per bus. For example, in Fig. 25a, which refers to the case of 75% of passengers in the system, i.e., nine passengers per bus, there are six peaks, each one in multiples of nine, plus some bars corresponding to numbers a little bit higher than the closest multiple of nine. This is explained by the fact that buses could serve not only passengers, but also pedestrians, totalizing a number of served links equal to the number of passengers plus a small number of pedestrians.

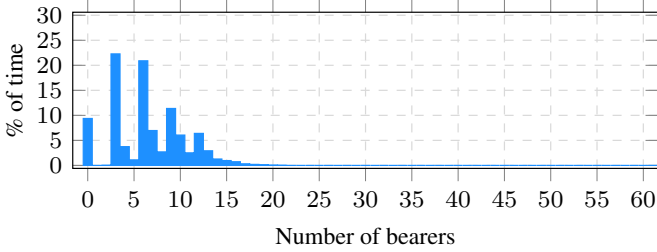
Finally, Fig. 26 presents the histograms of the percentage of links served by the IAB donors that correspond to access links. The complementary of these numbers corresponds to backhaul links. Remark that the percentage of links that are access



(a) 75% of passengers.



(b) 50% of passengers.



(c) 25% of passengers.

Fig. 25. Histogram of the number of links in the backhaul served by macro gNBs.

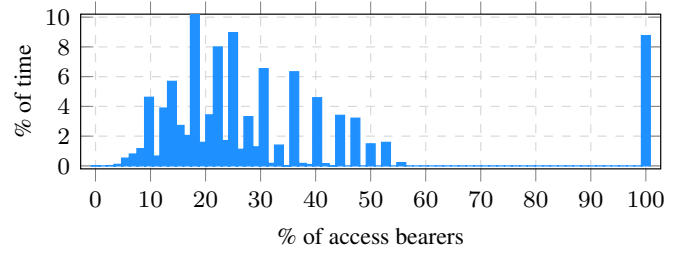
links varies a lot. As a consequence, one can conclude that adopting fixed time/frequency resources multiplexing schemes between donors and nodes may waste resources. For example, when the percentage of access links served by the IAB donor was low, it could be better to schedule more resources to the backhaul of connected mIAB nodes. In other words, one should consider adopting dynamic time/frequency resource multiplexing between access and backhaul based on the type of served links.

Based on the conclusions drawn in this section and on the concepts presented until now, next section summarizes the main learned lessons and points out open issues and possible directions to address them.

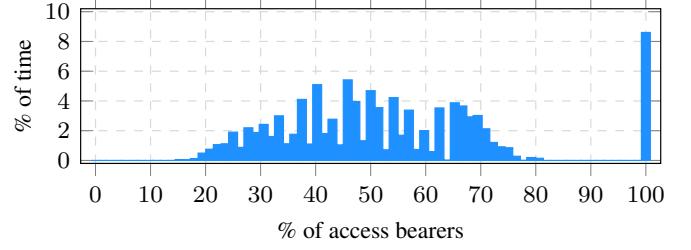
VI. LESSONS LEARNED, OPEN ISSUES AND FUTURE DIRECTIONS

A. Cell Planning

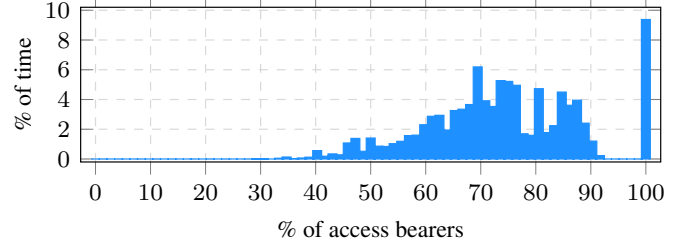
The mIAB state-of-the-art works which consider transports with previously known behavior, e.g., trains and buses, usually take advantage of that and deploy IAB donors in strategic places, e.g., along the railway track. For systems without a well-defined behavior, e.g., vehicles moving in a city, it is more challenging to design the system in advance, e.g., to define where the IAB donors should be deployed and how resource allocation and interference management



(a) 75% of passengers.



(b) 50% of passengers.



(c) 25% of passengers.

Fig. 26. Histogram of the percentage of links served by the macro gNBs that are access links.

can be handled. A promising direction is to adopt artificial intelligence (AI)-based solutions to learn possible mIAB node trajectories and how the traffic varies along the day in order to be able to deploy IAB donors in strategic positions.

B. Mobility Management

A challenge imposed by the mobility of an mIAB node is that it can suddenly overload its target IAB donor if the donor is not prepared to receive this new mIAB node. Similar to the previous topic, one adopted approach to deal with the mobility of mIAB nodes is to exploit the knowledge of the transport position and its trajectory, e.g., where a train or bus is and when they are going to arrive at the station. It allows the system to configure in advance the next IAB donor to receive the incoming UEs. However, this strategy is more challenging when we deal with vehicles without a well-defined trajectory. A promising solution to investigate is also to use prediction-based methods in those cases. For example, if the system is able to predict the arrival of an mIAB node, and its corresponding additional traffic, instants before it arrives, nearby BSs can perform load balancing in advance in order to reserve resources for the coming node.

C. Dynamic Interference Management

Whether interference management is required or not depends on different parameters such as the mIAB transmit

power, scheduling, power adaptation capability of the nodes, etc. Many works considered the access link provided by mIAB nodes deployed in a frequency spectrum different from the one used by the rest of the system in order to eliminate the interference caused by the mobility of those UEs through the system. This is not an efficient solution since the spectrum is expensive and scarce and might stay unused in a given area as long as no mIAB node is there. On the other hand, it is still a challenge to deploy access and backhaul links at the same frequency band due to the dynamic interference caused by the mobility of the mIAB nodes. Thus, solutions for in-band interference management must be further investigated. For example, one can perform power control in the mIAB nodes access links in order to reduce/avoid interfering with nearby UEs connected to the IAB donor. Another option is to insert slots of silence on the TDD frame pattern, as investigated in [118].

D. Bandwidth Allocation for Access and Backhaul

Most of the works considering in-band deployment of mIAB adopted a fixed split of the resource (either in frequency or in time) between access and backhaul link. A strategy for sharing resources between backhaul link and access links of inside and outside UEs is still a challenge and must be further investigated, since it can lead to more efficient use of the spectrum. For example, dynamic spectrum partitioning could be performed taking into account the load of data to be transmitted in the backhaul and in the access links of IAB donor and mIAB nodes. This solution guarantees fairness and avoids the waste of resources in case part of the spectrum is reserved for a given type of link, e.g., backhaul, but there is not enough data to be transmitted in that link.

E. Antenna Deployment

It is almost a consensus that at least for trains and buses antennas are going to be deployed outside and at the top of these transports being connected to inside APs which will provide connectivity for inside UEs. However, practical considerations must still be further evaluated, e.g., each operator will need to deploy its own equipment or will the infrastructure be shared, e.g., computational resources, antennas and frequency spectrum. Moreover, since a possible use case of mIAB nodes is to serve not only onboard UEs but also surrounding UEs, it is important to evaluate and compare pros and cons of deploying DU antennas either only inside or both inside and outside of mIAB nodes.

F. Role of UAV

UAV-based communication is not considered in 3GPP Release 18 work-item on mIAB. However, from an academic perspective, it is still interesting to investigate its performance. Works which use UAVs to enhance the coverage of the network usually first define an optimal position for the UAVs and fix them there. It is still under evaluated how UAVs perform when continually moving either to provide access link for UEs or to provide a wireless backhaul for other IABs nodes.

G. Improved Reliability for C-plane

3GPP standard documents do not yet cover mIAB aspects. Different aspects should still be investigated, e.g., the possibility of splitting user and control planes as in dual connectivity (DC) scenarios. In the context of mIAB U-plane could be multi-hop while C-plane would be one-hop [119]. This approach aims at reducing latency and failure probability. Furthermore, U/C-planes could even be deployed at different frequencies, where U-plane would be deployed at mmWave for enhanced throughput while C-plane would be deployed at C-band for higher reliability and coverage.

H. Topology Adaptation on mobile IAB

With inter-CU topology adaptation, an IAB node migrates from an old parent to a new parent where both parent nodes are served by different IAB donor CUs. The current discussions are about the need for both MT and DU parts of the migrating IAB node to handover. The main point is that DU migration requires that all child nodes and UEs should perform handover to the new target donor-CU. This is not the case when only MT-part handover is executed. DU migration involves context transfer of the child IAB nodes and UEs, update of their security keys and causes a large amount of signaling to be exchanged via the Xn, F1 and radio interfaces [120]. This flood of signaling is called signaling storm. The main concern is that this procedure may cause service interruption as, currently, each DU can be connected simultaneously to only one CU. One of the envisaged solutions is the possibility of the support of two logical DUs, but this may increase the complexity of IAB. Although these discussions on 3GPP are focused on fixed IAB, they certainly are of utmost relevance for future discussions on mIAB where topology adaptation should be more frequent.

I. Signaling Optimization for Group Handover

Another important aspect that has been discussed on 3GPP meetings is about the optimization of group handover when the DU part changes its parent in inter-CU topology adaptation. If standard handover procedure is followed, all child nodes and UEs would perform Xn handover procedure including the random access (RACH) procedure. However, note that the RACH procedure is not necessary in these cases since there is no change in the UE's strongest cell and child IAB nodes' strongest parent. Finally, group signaling could be tailored for this case where handover messages of several UEs could be concatenated/compressed [121]. As an example, each UE's RRC reconfiguration message could be significantly reduced by updating only few parameters.

VII. CONCLUSIONS

As presented in this work, mIAB is a candidate solution to address at least two challenges of current networks. Firstly, it enhances the service of moving UEs, e.g., passengers of trains and buses, guaranteeing that they are always connected and avoiding overloading the network with HO messages when a group of moving UEs enters simultaneously the coverage area

of a new cell. Secondly, it allows a quick deployment of new cells to provide/improve connectivity in high demanding areas with the deployment of mIAB nodes.

The basis for the deployment of mIAB were presented. They are: current status of IAB standardization in 5G NR and state-of-the-art works regarding fixed IAB and mIAB. In order to help readers interested in this subject, the state-of-the-art works were classified following different criteria. On the one hand, fixed mobile related works were classified according to the studied dimensions, system modeling assumptions/constraints, considered problem objectives and KPIs, solution approaches and adopted mathematical tools. On the other hand, mIAB related works were grouped according to the type of mobility, e.g., train, bus, UAV, etc.. It was noticed that works considering similar type of mobility usually consider similar problems, e.g., UAV positioning, and take advantage of specific characteristics of each type of mobility, e.g., previously known mobile trajectory of buses.

After the literature review, we have performed an extensive analysis of mIAB based on computational simulations. It was considered an urban macro scenario where IAB nodes were deployed in buses in order to improve the passengers' connection. It was presented passengers and pedestrians throughput, latency and link quality in both downlink and uplink transmission directions. Results related to the wireless backhaul were also presented as well as the profile of links served by the IAB donors. It was concluded that the deployment of the DU part of an IAB node inside a bus and its MT part outside the bus remarkably improves the passengers throughput and latency. This is due to the fact that this deployment overcomes the significant bus penetration loss that a link between a BS outside the bus and a passenger suffers. Moreover, it was also concluded that an admission policy to allow a UE to connect to a mIAB cell should be adopted. The admission criteria could be: a minimum measured RSRP value; a maximum measured interference level (RSRQ instead of RSRP); the relative UE and bus geographical position in a given time interval; etc.. Furthermore, it was concluded that the adopted topology adaptation and TDD scheme play an important role directly impacting the interference management strategy. Thus, it would be better if dynamic topology adaptation and time/frequency resource scheduling were adopted taking into account the IAB donor load, e.g., amount of served traffic from access and backhaul links.

Finally, we have summarized lessons learned, open issues and future directions related to mIAB. One important challenge is how to deal with the dynamic interference caused by mobile cells when moving around the system, specially in the case with in-band deployment of backhaul and access. Besides, a promising solution for this and other challenges is the use of predictive solutions, e.g., AI-based, in order to anticipate what is going to happen and prepare the system in advance.

REFERENCES

- [1] V. Jungnickel, K. Manolakis, W. Zirwas, B. Panzner, V. Braun, M. Lossow, M. Sternad, R. Apelfröjd, and T. Svensson, "The role of small cells, coordinated multipoint, and massive mimo in 5G," *IEEE Commun. Mag.*, vol. 52, no. 5, pp. 44–51, May 2014. DOI: 10.1109/MCOM.2014.6815892.
- [2] S. Dang, O. Amin, B. Shihada, and M.-S. Alouini, "What should 6G be?" *Nature Electron.*, no. 3, pp. 20–29, Jan. 2020. DOI: 10.1038/s41928-019-0355-6.
- [3] T. Inoue, "5G NR release 16 and millimeter wave integrated access and backhaul," in *Proc. of the IEEE Radio and Wireless Symp. (RWS)*, San Antonio, TX, USA, Jan. 2020, pp. 56–59. DOI: 10.1109/RWS45077.2020.9050108.
- [4] W. Ni and I. B. Collings, "A new adaptive frequency allocation algorithm in multi-hop point-to-point FDD backhaul networks for metro cells," in *Proc. of the Internat. Symp. on Commun. and Inf. Tech. (ISCIT)*, Gold Coast, Australia, Oct. 2012, pp. 187–192. DOI: 10.1109/ISCIT.2012.6380887.
- [5] H. S. Dhillon and G. Caire, "Scalability of line-of-sight massive MIMO mesh networks for wireless backhaul," in *Proc. of the IEEE Internat. Symp. on Inf. Theory*, Honolulu, HI, USA, Jun. 2014, pp. 2709–2713. DOI: 10.1109/ISIT.2014.6875326.
- [6] D. Schulz, M. Schlosser, C. Alexakis, K. H. Jonas, Hilt, R. Freund, and V. Jungnickel, "Optical wireless LED link for the backhaul of small cells," in *Proc. of the Optical Fiber Commun. Conf. and Exhib. (OFC)*, Los Angeles, CA, USA, Mar. 2015, pp. 1–3. DOI: 10.1364/OFC.2015.M2F.8.
- [7] T. F. Rahman, C. Sacchi, and C. Stallo, "MM-wave LTE-A small-cell wireless backhauling based on TH-IR techniques," in *Proc. of the IEEE Aerosp. Conf.*, Montana, USA, Mar. 2015, pp. 1–9. DOI: 10.1109/AERO.2015.7118906.
- [8] B. Yin, N. Wang, Y. Fan, X. Sun, D. He, and W. Liu, "Evaluation of TDM-based integrated access and backhaul schemes for 5G and beyond at mmWave band," in *Proc. of the Internat. Conf. on Cyber-Enabled Distrib. Comput. and Knowl. Discovery (CyberC)*, Chongqing, China, Oct. 2020, pp. 348–353. DOI: 10.1109/CyberC49757.2020.00065.
- [9] W. Xi, N.-T. Mao, and K. Rundberget, "Cost comparisons of backhaul transport technologies for 5G fixed wireless access," in *Proc. of IEEE 5G World Forum (5GWF)*, Santa Clara, CA, USA, Jul. 2018, pp. 159–163. DOI: 10.1109/5GWF.2018.8516977.
- [10] Y. Zhang, M. A. Kishk, and M.-S. Alouini, "A survey on integrated access and backhaul networks," *Frontiers in Commun. and Netw.*, vol. 2, pp. 1–24, Jun. 2021, ISSN: 2673-530X. DOI: 10.3389/frcmn.2021.647284.
- [11] S. Jaffry, R. Hussain, X. Gui, and S. F. Hasan, "A comprehensive survey on moving networks," *IEEE Commun. Surveys Tuts.*, vol. 23, no. 1, pp. 110–136, Oct. 2021. DOI: 10.1109/COMST.2020.3029005.
- [12] 3GPP, "Overview of 3GPP Release 16," 3rd Generation Partnership Project (3GPP), TR. Jul. 2014. [Online]. Available: https://www.3gpp.org/ftp/Information/WORK_PLAN/Description_Releases/.
- [13] —, "Evolved Universal Terrestrial Radio Access (E-UTRA); Relay architectures for E-UTRA (LTE-Advanced)," 3rd Generation Partnership Project (3GPP), TR 36.806, Apr. 2010. [Online]. Available: <http://www.3gpp.org/ftp/Specs/html-info/36806.htm>.
- [14] M. Polese, M. Giordani, T. Zugno, A. Roy, S. Goyal, D. Castor, and M. Zorzi, "Integrated access and backhaul in 5G mmWave networks: Potential and challenges," *IEEE Commun. Mag.*, vol. 58, no. 3, pp. 62–68, Mar. 2020. DOI: 10.1109/MCOM.001.1900346.
- [15] 3GPP, "NR; study on integrated access and backhaul (release 16)," 3rd Generation Partnership Project (3GPP), TR 38.874, Dec. 2018, v.16.0.0. [Online]. Available: <http://www.3gpp.org/ftp/Specs/html-info/38874.htm> (visited on 04/13/2021).
- [16] —, "NR; NR and NG-RAN Overall description; Stage 2," 3rd Generation Partnership Project (3GPP), TS 38.300, Sep. 2020, v.16.3.0. [Online]. Available: <http://www.3gpp.org/ftp/Specs/html-info/38300.htm> (visited on 04/13/2021).
- [17] —, "NR; integrated access and backhaul radio transmission and reception," 3rd Generation Partnership Project (3GPP), TS 38.174, Dec. 2020, v.16.1.0. [Online]. Available: <http://www.3gpp.org/ftp/Specs/html-info/38174.htm> (visited on 04/13/2021).
- [18] C. Madapatha, B. Makki, C. Fang, O. Teyeb, E. Dahlman, M.-S. Alouini, and T. Svensson, "On integrated access and backhaul networks: Current status and potentials," *IEEE Open J. Commu. Soc.*, vol. 1, pp. 1374–1389, Sep. 2020. DOI: 10.1109/OJCOMS.2020.3022529.
- [19] 3GPP, "NG-RAN; F1 general aspects and principles (Release 16)," 3rd Generation Partnership Project (3GPP), TS 38.470, Apr. 2021, v.16.4.0. [Online]. Available: https://www.3gpp.org/ftp/Specs/archive/38_series/38.470/38470-g40.zip (visited on 04/18/2021).

- [20] —, “NR; Backhaul Adaptation Protocol (BAP) specification (Release 16),” 3rd Generation Partnership Project (3GPP), TS 38.340, Mar. 2021, v.16.4.0. [Online]. Available: <http://www.3gpp.org/ftp/Specs/html-info/38340.htm> (visited on 04/15/2021).
- [21] —, “NG-RAN; Architecture description,” 3rd Generation Partnership Project (3GPP), TS 38.401, Sep. 2020, v.16.3.0. [Online]. Available: <http://www.3gpp.org/ftp/Specs/html-info/383401.htm> (visited on 04/14/2021).
- [22] E. Dhalman, S. Parkvall, and J. Skold, *5G NR The Next Generation Wireless Access Technology*. Mara Conner, 2021, ISBN: 978-0-12-822320-8.
- [23] 3GPP, “New WID on Enhancements to Integrated Access and Backhaul,” 3rd Generation Partnership Project (3GPP), RP 210758, Mar. 2021, Meeting no. 91e. [Online]. Available: https://www.3gpp.org/tp/TSG_RAN/TSG_RAN/TSGR_91e/DocsRP-210758.zip (visited on 04/18/2021).
- [24] E. Dhalman, S. Parkvall, and J. Skold, *5G NR The Next Generation Wireless Access Technology*, 2nd ed. Mara Conner, 2021, ISBN: 978-0-12-822320-8.
- [25] O. Teyeb, A. Muhammad, G. Mildh, E. Dahlman, F. Barac, and B. Makki, “Integrated access backhauled networks,” in *Proc. of the IEEE Vehic. Tech. Conf. (VTC)*, Honolulu, HI, USA, Nov. 2019, pp. 1–5. DOI: 10.1109/VTCSFall.2019.8891507.
- [26] H. Ronkainen, J. Edstam, A. Ericsson, and C. Östberg, “Integrated access and backhaul – a new type of wireless backhaul in 5G,” Ericsson, Stockholm, Sweden, Technical Report 7, Jun. 2020, pp. 2–11. [Online]. Available: <https://www.ericsson.com/en/reports-and-papers/ericsson-technology-review/articles/introducing-integrated-access-and-backhaul> (visited on 09/20/2021).
- [27] C. Madapatha, B. Makki, A. Muhammad, E. Dahlman, M.-S. Alouini, and T. Svensson, “On topology optimization and routing in integrated access and backhaul networks: A genetic algorithm-based approach,” *IEEE Open J. Commu. Soc.*, vol. 2, pp. 2273–2291, Sep. 2021. DOI: 10.1109/OJCOMS.2021.3114669.
- [28] H. Ronkainen, J. Edstam, A. Ericsson, and C. Östberg, “Integrated access and backhaul: A new type of wireless backhaul in 5g,” *Frontiers in Commun. and Netw.*, vol. 2, Apr. 2021, ISSN: 2673-530X. DOI: 10.3389/frcmn.2021.636949.
- [29] J. Zhang, N. Garg, M. Holm, and T. Ratnarajah, “Design of full duplex millimeter-wave integrated access and backhaul networks,” *IEEE Wireless Commun.*, vol. 28, no. 1, pp. 60–67, Feb. 2021. DOI: 10.1109/MWC.001.2000199.
- [30] M. Cudak, A. Ghosh, A. Ghosh, and J. Andrews, “Integrated access and backhaul: A key enabler for 5g millimeter-wave deployments,” *IEEE Commun. Mag.*, vol. 59, no. 4, pp. 88–94, May 2021. DOI: 10.1109/MCOM.001.2000690.
- [31] T. Tian, Y. Dou, G. Ren, L. Gu, J. Chen, Y. Cui, T. Takada, M. Iwabuchi, J. Tsuboi, and Y. Kishiyama, “Field trial on millimeter wave integrated access and backhaul,” in *Proc. of the IEEE Vehic. Tech. Conf. (VTC)*, Kuala Lumpur, Malaysia, Apr. 2019, pp. 1–5. DOI: 10.1109/VTCSpring.2019.8746375.
- [32] M. Polese, M. Giordani, A. Roy, S. Goyal, D. Castor, and M. Zorzi, “End-to-end simulation of integrated access and backhaul at mmWaves,” in *Proc. of the IEEE Internat. Workshop on Comput. Aided Modeling and Design of Commun. Links and Netw. (CAMAD)*, Barcelona, Spain, Nov. 2018, pp. 1–7. DOI: 10.1109/CAMAD.2018.8514996.
- [33] M. N. Islam, N. Abedini, G. Hampel, S. Subramanian, and J. Li, “Investigation of performance in integrated access and backhaul networks,” in *Proc. of the IEEE Conf. on Comput. Commun. (INFOCOM)*, Honolulu, HI, USA, Jul. 2018, pp. 597–602. DOI: 10.1109/INFOCOMW.2018.8406872.
- [34] C. Saha and H. S. Dhillon, “Millimeter wave integrated access and backhaul in 5G: Performance analysis and design insights,” *IEEE J. Sel. Areas Commun.*, vol. 37, no. 12, pp. 2669–2684, Oct. 2019. DOI: 10.1109/JSAC.2019.2947997.
- [35] S. Ranjan, P. Chaporkar, P. Jha, and A. Karandikar, “Backhaul-aware cell selection policies in 5g iab networks,” in *Proc. of the IEEE Wireless Commun. and Netw. Conf. (WCNC)*, Nanjing, China, May 2021, pp. 1–6. DOI: 10.1109/WCNC49053.2021.9417398.
- [36] M. Polese, M. Giordani, A. Roy, D. Castor, and M. Zorzi, “Distributed path selection strategies for integrated access and backhaul at mmwaves,” in *Proc. of the IEEE Global Telecommun. Conf. (GLOBECOM)*, Abu Dhabi, United Arab Emirates, Dec. 2018, pp. 1–7. DOI: 10.1109/GLOCOM.2018.8647977.
- [37] M. E. Rasekh, D. Guo, and U. Madhow, “Joint routing and resource allocation for millimeter wave picocellular backhaul,” *IEEE Trans. Wireless Commun.*, vol. 19, no. 2, pp. 783–794, Oct. 2020. DOI: 10.1109/TWC.2019.2948624.
- [38] —, “Interference-aware routing and spectrum allocation for millimeter wave backhaul in urban picocells,” in *Proc. of Allerton Conf. on Commun., Control, and Comput. (Allerton)*, Monticello, IL, USA, Sep. 2015, pp. 1–7. DOI: 10.1109/ALLERTON.2015.7557347.
- [39] E. Arribas, A. Fernández Anta, D. R. Kowalski, V. Mancuso, M. A. Mosteiro, J. Widmer, and P. W. H. Wong, “Optimizing mmwave wireless backhaul scheduling,” *IEEE Trans. Mobile Comput.*, vol. 19, no. 10, pp. 2409–2428, Oct. 2020. DOI: 10.1109/TMC.2019.2924884.
- [40] M. Simsek, M. Narasimha, O. Orhan, H. Nikopour, W. Mao, and S. Talwar, “Optimal topology formation and adaptation of integrated access and backhaul networks,” *Frontiers in Commun. and Netw.*, vol. 1, pp. 1–12, Jan. 2021, ISSN: 2673-530X. DOI: 10.3389/frcmn.2020.608088.
- [41] T. K. Vu, M. Bennis, M. Debbah, and M. Latva-Aho, “Joint path selection and rate allocation framework for 5g self-backhauled mm-wave networks,” *IEEE Trans. Wireless Commun.*, vol. 18, no. 4, pp. 2431–2445, Mar. 2019. DOI: 10.1109/TWC.2019.2904275.
- [42] Y. Li, J. Luo, R. A. Stirling-Gallacher, and G. Caire. (Jan. 2019). “Integrated access and backhaul optimization for millimeter wave heterogeneous networks.” arXiv: 1901.04959 [cs.IT].
- [43] A. HasanzadeZonuzi, I. Hou, and S. Shakkottai, “Broadcasting real-time flows in integrated backhaul and access 5g networks,” in *Proc. of the Internat. Symp. on Modeling and Opt. in Mobile, Ad Hoc, and Wireless Netw. (WiOPT)*, Avignon, France, Jul. 2019, pp. 1–8. DOI: 10.23919/WiOPT47501.2019.9144141.
- [44] B. Zhai, M. Yu, A. Tang, and X. Wang, “Mesh architecture for efficient integrated access and backhaul networking,” in *Proc. of the IEEE Wireless Commun. and Netw. Conf. (WCNC)*, Seoul, South Korea, May 2020, pp. 1–6. DOI: 10.1109/WCNC45663.2020.9120546.
- [45] Q. Zhang, K. Luo, W. Wang, and T. Jiang, “Joint c-oma and c-noma wireless backhaul scheduling in heterogeneous ultra dense networks,” *IEEE Trans. Wireless Commun.*, vol. 19, no. 2, pp. 874–887, Nov. 2020. DOI: 10.1109/TWC.2019.2949791.
- [46] J. Y. Lai, W.-H. Wu, and Y. T. Su, “Resource allocation and node placement in multi-hop heterogeneous integrated-access-and-backhaul networks,” *IEEE Access*, vol. 8, pp. 122937–122958, Jul. 2020. DOI: 10.1109/ACCESS.2020.3007501.
- [47] M. Al-Jarrah, E. Alsusa, A. Al-Dweik, and M.-S. Alouini, “Performance analysis of wireless mesh backhauling using intelligent reflecting surfaces,” *IEEE Trans. Wireless Commun.*, pp. 1–1, Jun. 2021. DOI: 10.1109/TWC.2021.3052370.
- [48] C. Fang, C. Madapatha, B. Makki, and T. Svensson, “Joint scheduling and throughput maximization in self-backhauled millimeter wave cellular networks,” in *Proc. of the Internat. Symp. on Wireless Commun. Syst. (ISWCS)*, Berlin, Germany, Sep. 2021, pp. 1–6. DOI: 10.1109/ISWCS49558.2021.9562232.
- [49] C. Saha, M. Afshang, and H. S. Dhillon, “Integrated mmWave access and backhaul in 5G: Bandwidth partitioning and downlink analysis,” in *Proc. of the IEEE Internat. Conf. on Commun. (ICC)*, Jul. 2018, pp. 1–6. DOI: 10.1109/ICC.2018.8422149.
- [50] C. Saha, M. Afshang, and H. S. Dhillon, “Bandwidth partitioning and downlink analysis in millimeter wave integrated access and backhaul for 5g,” *IEEE Trans. Wireless Commun.*, vol. 17, no. 12, pp. 8195–8210, Dec. 2018. DOI: 10.1109/TWC.2018.2874655.
- [51] G. Kwon and H. Park, “Joint user association and beamforming design for millimeter wave UDN with wireless backhaul,” *IEEE J. Sel. Areas Commun.*, vol. 37, no. 12, pp. 2653–2668, Oct. 2019. DOI: 10.1109/JSAC.2019.2947926.
- [52] Y. Liu, A. Tang, and X. Wang, “Joint incentive and resource allocation design for user provided network under 5g integrated access and backhaul networks,” *IEEE Trans. Netw. Sci. Eng.*, vol. 7, no. 2, pp. 673–685, Apr. 2020. DOI: 10.1109/TNSE.2019.2910867.
- [53] H. Zheng and L. Li, “Joint backhaul bandwidth and power allocation in heterogeneous cellular networks: A two-level approach,” *Internat. J. of Commun. Syst.*, vol. 33, no. 11, Apr. 2020. DOI: 10.1002/dac.4420.
- [54] A. J. Muhammed, Z. Ma, Z. Zhang, P. Fan, and E. G. Larsson, “Energy-efficient resource allocation for NOMA based small cell networks with wireless backhauled,” *IEEE Trans. Commun.*, vol. 68, no. 6, pp. 3766–3781, Mar. 2020. DOI: 10.1109/TCOMM.2020.2979971.
- [55] W. Lei, Y. Ye, and M. Xiao, “Deep reinforcement learning-based spectrum allocation in integrated access and backhaul networks,”

- IEEE Trans. on Cogn. Commun. Netw.*, vol. 6, no. 3, pp. 970–979, May 2020. DOI: 10.1109/TCCN.2020.2992628.
- [56] M. Pagin, T. Zugno, M. Polese, and M. Zorzi, “Resource management for 5G NR integrated access and backhaul: A semi-centralized approach,” *IEEE Trans. Wireless Commun.*, vol. 21, no. 2, pp. 753–767, 2022. DOI: 10.1109/TWC.2021.3098967.
- [57] H. Alghafari and M. S. Haghighi, “Decentralized joint resource allocation and path selection in multi-hop integrated access backhaul 5g networks,” *Comput. Netw.*, vol. 207, p. 108837, 2022, ISSN: 1389-1286.
- [58] S. Gopalram, S. V. Hanly, and P. Whiting, “Distributed and local scheduling algorithms for mmwave integrated access and backhaul,” *IEEE/ACM Trans. Netw.*, pp. 1–16, 2022. DOI: 10.1109/TNET.2022.3154367.
- [59] O. P. Adare, H. Babbili, C. Madapatha, B. Makki, and T. Svensson. (Oct. 2021). “Uplink power control in integrated access and backhaul networks.” arXiv: 2110.07704 [cs.NI].
- [60] E. Xue, X. Tao, and N. Zhang, “User-centric joint access-backhaul design for full-duplex self-backhauled wireless networks,” *IEEE Trans. Commun.*, vol. 67, no. 11, pp. 7980–7993, Aug. 2019. DOI: 10.1109/TCOMM.2019.2932987.
- [61] Y. Xue, X. Zheng, and V. K. N. Lau, “Line-of-sight mimo for high capacity millimeter wave backhaul in fdd systems,” *J. of Commun. and Inf. Netw.*, vol. 5, no. 2, pp. 177–193, Jun. 2020. DOI: 10.23919/JCIN.2020.9130434.
- [62] Y. Sadovaya, D. Moltchanov, H. Nikopour, S.-p. Yeh, W. Mao, O. Orhan, S. Talwar, and S. Andreev, “Self-interference assessment and mitigation in 3gpp iab deployments,” in *Proc. of the IEEE Internat. Conf. on Commun. (ICC)*, Virtual Conference, Aug. 2021, pp. 1–6. DOI: 10.1109/ICC42927.2021.9500769.
- [63] J. Zhang, H. Luo, N. Garg, M. Holm, and T. Ratnarajah, “Design and analysis of mmwave full-duplex integrated access and backhaul networks,” in *Proc. of the IEEE Internat. Conf. on Commun. (ICC)*, Virtual Conference, Jun. 2021, pp. 1–6. DOI: 10.1109/ICC42927.2021.9500615.
- [64] 3GPP, “Mobile Relay for E-UTRA,” 3rd Generation Partnership Project (3GPP), TR 36.836, Oct. 2012. [Online]. Available: <http://www.3gpp.org/ftp/Specs/html-info/36836.htm>.
- [65] —, “Study on vehicle-mounted relays; stage 1 (release 18),” 3rd Generation Partnership Project (3GPP), TR 22.839, Sep. 2021, v.18.0.0. [Online]. Available: <http://www.3gpp.org/ftp/Specs/html-info/22839.htm> (visited on 10/20/2021).
- [66] J. Wu and P. Fan, “A survey on high mobility wireless communications: Challenges, opportunities and solutions,” *IEEE Access*, vol. 4, pp. 450–476, Jan. 2016. DOI: 10.1109/ACCESS.2016.2518085.
- [67] B. Ai, A. F. Molisch, M. Rupp, and Z. -Z. Zhong, “5g key technologies for smart railways,” *Proc. IEEE*, vol. 108, no. 6, pp. 856–893, Jun. 2020. DOI: 10.1109/JPROC.2020.2988595.
- [68] P. T. Dat, A. Kanno, K. Inagaki, F. Rottenberg, N. Yamamoto, and T. Kawanishi, “High-speed and uninterrupted communication for high-speed trains by ultrafast WDM fiber-wireless backhaul system,” *J. Lightw. Technol.*, vol. 37, no. 1, pp. 205–217, Jan. 2019. DOI: 10.1109/JLT.2018.2885548.
- [69] J. Xu and B. Ai, “Artificial intelligence empowered power allocation for smart railway,” *IEEE Commun. Mag.*, vol. 59, no. 2, pp. 28–33, Feb. 2021. DOI: 10.1109/MCOM.001.2000634.
- [70] Y. Lu, K. Xiong, P. Fan, Z. Zhong, and B. Ai, “The effect of power adjustment on handover in high-speed railway communication networks,” *IEEE Access*, vol. 5, pp. 26237–26250, Nov. 2017. DOI: 10.1109/ACCESS.2017.2775044.
- [71] A. Gonzalez-Plaza, J. Moreno, I. Val, A. Arriola, P. M. Rodriguez, F. Jimenez, and C. Briso, “5G communications in high speed and metropolitan railways,” in *Proc. of the European Conf. on Antennas and Prop.*, Paris, France, Mar. 2017, pp. 658–660. DOI: 10.23919/EuCAP.2017.7928756.
- [72] M. Choi, B. Yoon, D. Kim, and D. Sung, “IAB-based railway communication method for stable service provision,” in *Proc. of the Internat. Conf. on Ubiquitous and Fut. Netw. (ICUFN)*, Jeju Island, Korea and Virtual Conference, Aug. 2021, pp. 176–178. DOI: 10.1109/ICUFN49451.2021.9528777.
- [73] M. Ichinose and I. Nakagawa, “Verification trials of 5G communications in high-speed mobile environments,” *New Breeze*, vol. 30, no. 4, pp. 6–8, Oct. 2018, ISSN: 0915-3160.
- [74] M. Gao, B. Ai, Y. Niu, W. Wu, P. Yang, F. Lyu, and X. Shen, “Efficient hybrid beamforming with anti-blockage design for high-speed railway communications,” *IEEE Trans. Veh. Technol.*, vol. 69, no. 9, pp. 9643–9655, Sep. 2020. DOI: 10.1109/TVT.2020.3000757.
- [75] H. Guo, B. Makki, D.-T. Phan-Huy, E. Dahlman, M.-S. Alouini, and T. Svensson, “Predictor antenna: A technique to boost the performance of moving relays,” *IEEE Commun. Mag.*, vol. 59, no. 7, pp. 80–86, Jul. 2021. DOI: 10.1109/MCOM.001.2001205.
- [76] H. Guo, B. Makki, M.-S. Alouini, and T. Svensson, “On delay-limited average rate of HARQ-based predictor antenna systems,” *IEEE Wireless Commun. Lett.*, vol. 10, no. 8, pp. 1628–1632, Aug. 2021. DOI: 10.1109/LWC.2021.3075351.
- [77] —, (Sep. 2021). “High-rate uninterrupted internet-of-vehicle communications in highways: Dynamic blockage avoidance and CSIT acquisition.” arXiv: 2109.12878, (visited on 01/03/2022).
- [78] D.-T. Phan-Huy, S. Wesemann, J. Bjorsell, and M. Sternad, “Adaptive massive mimo for fast moving connected vehicles: It will work with predictor antennas!” In *22nd International ITG Workshop on Smart Antennas*, Mar. 2018, pp. 1–8.
- [79] Y. Sui, A. Papadogiannis, W. Yang, and T. Svensson, “Performance comparison of fixed and moving relays under co-channel interference,” in *Proc. of the IEEE Global Telecommun. Conf. Workshops (GLOBECOM Workshops)*, Anaheim, CA, USA, Dec. 2012, pp. 574–579. DOI: 10.1109/GLOCOMW.2012.6477637.
- [80] Y. Sui, A. Papadogiannis, and T. Svensson, “The potential of moving relays - a performance analysis,” in *Proc. of the IEEE Vehic. Tech. Conf. (VTC)*, Yokohama, Japan, Jul. 2012, pp. 1–5. DOI: 10.1109/VETCS.2012.6240247.
- [81] Y. Sui, A. Papadogiannis, W. Yang, and T. Svensson, “The energy efficiency potential of moving and fixed relays for vehicular users,” in *Proc. of the IEEE Vehic. Tech. Conf. (VTC)*, Las Vegas, NV, USA, Sep. 2013, pp. 1–7. DOI: 10.1109/VTCFall.2013.6692436.
- [82] J. Gui and X. Dai, “Stabilizing mmWave backhaul energy efficiency for vehicle-mounted access points by Q-learning-based scheme,” *Wireless Personal Commun.*, Aug. 2021. DOI: 10.1007/s11277-021-08854-w.
- [83] S. Jangsher and V. O. K. Li, “Backhaul resource allocation for existing and newly arrived moving small cells,” *IEEE Trans. Veh. Technol.*, vol. 66, no. 4, pp. 3211–3219, Apr. 2017. DOI: 10.1109/TVT.2016.2590502.
- [84] S. Jaffry, S. F. Hasan, and X. Gui, “Efficient resource-sharing algorithms for mobile-cell’s sidehaul and access links,” *IEEE Networking Letters*, vol. 1, no. 2, pp. 72–75, Feb. 2019. DOI: 10.1109/LNET.2019.2899870.
- [85] S. Jaffry, S. F. Hasan, and X. Gui, “Interference management and resource sharing in moving networks,” *IET Commun.*, vol. 13, no. 16, pp. 2580–2589, Oct. 2019. DOI: 10.1049/iet-com.2018.6193.
- [86] S. Jaffry, S. F. Hasan, and X. Gui, “Shared spectrum for mobile-cell’s backhaul and access link,” in *Proc. of the IEEE Global Telecommun. Conf. (GLOBECOM)*, Abu Dhabi, United Arab Emirates, Dec. 2018, pp. 1–6. DOI: 10.1109/GLOCOM.2018.8647131.
- [87] S. Jaffry, S. F. Hasan, and X. Gui. (Aug. 2018). “Effective resource sharing in mobile-cell environments.” arXiv: 1808.01700 [eess.SP].
- [88] A. Jaziri, R. Nasri, and T. Chahed, “Offloading traffic hotspots using moving small cells,” in *Proc. of the IEEE Internat. Conf. on Commun. (ICC)*, Kuala Lumpur, Malaysia, May 2016, pp. 1–6. DOI: 10.1109/ICC.2016.7511566.
- [89] A. Mastro Simone and D. Panno, “New challenge: Moving network based on mmWave technology for 5G era,” in *Proc. of the Internat. Conf. on Comput., Inf. and Telecommun. Syst. (CITS)*, Gijon, Spain, Oct. 2015, pp. 1–5. DOI: 10.1109/CITS.2015.7297756.
- [90] A. Mastro Simone and D. Panno, “A comparative analysis of mmwave vs lte technology for 5g moving networks,” in *Proc. of the IEEE Wireless and Mob. Comput., Network. and Commun. (WiMob)*, Abu Dhabi, United Arab Emirates, Dec. 2015, pp. 422–429. DOI: 10.1109/WiMOB.2015.7347993.
- [91] A. Mastro Simone and D. Panno, “Moving network based on mmWave technology: A promising solution for 5G vehicular users,” *Wireless Netw.*, vol. 24, no. 7, pp. 2409–2426, Mar. 2017. DOI: 10.1007/s11276-017-1479-0.
- [92] S. Chae, M. Z. Chowdhury, T. Nguyen, and Y. M. Jang, “A dynamic frequency allocation scheme for moving small-cell networks,” in *Proc. of the Internat. Conf. on ICT Convergence (ICTC)*, Jeju Island, Korea (South), Dec. 2012, pp. 125–128. DOI: 10.1109/ICTC.2012.6386795.
- [93] S. Jangsher and V. O. K. Li, “Resource allocation in cellular networks with moving small cells with probabilistic mobility,” in *Proc. of the IEEE Personal, Indoor and Mob. Radio Commun. (PIMRC)*,

- Washington, DC, USA, Jun. 2014, pp. 1701–1705. DOI: 10.1109/PIMRC.2014.7136442.
- [94] M. Z. Chowdhury, S. H. Chae, and Y. M. Jang, “Group handover management in mobile femtocellular network deployment,” in *Proc. of the Internat. Conf. on Ubiqu. and Fut. Netw. (ICUFN)*, Phuket, Thailand, Aug. 2012, pp. 162–165. DOI: 10.1109/ICUFN.2012.6261685.
- [95] R. Raheem, A. Lasebae, and J. Loo, “Performance evaluation of LTE network via using fixed/mobile femtocells,” in *Proc. of the Internat. Conf. on Adv. Inf. Netw. and Appl. Workshops*, Victoria, Canada, May 2014, pp. 255–260. DOI: 10.1109/WAINA.2014.51.
- [96] M. Tayyab, G. P. Koudouridis, X. Gelabert, and R. Jäntti, “Handover performance and power consumption analysis of lte mobile relays,” in *Proc. of the IEEE Vehic. Tech. Conf. (VTC)*, Victoria, Canada, Nov. 2020, pp. 1–5. DOI: 10.1109/VTC2020-Fall49728.2020.9348720.
- [97] I. Bor-Yaliniz, M. Salem, G. Senerath, and H. Yanikomeroglu, “Is 5g ready for drones: A look into contemporary and prospective wireless networks from a standardization perspective,” *IEEE Wireless Commun.*, vol. 26, no. 1, pp. 18–27, Feb. 2019. DOI: 10.1109/MWC.2018.1800229.
- [98] M. Gapeyenko, V. Petrov, D. Moltchanov, S. Andreev, N. Himayat, and Y. Koucheryavy, “Flexible and reliable UAV-assisted backhaul operation in 5G mmWave cellular networks,” *IEEE J. Sel. Areas Commun.*, vol. 36, no. 11, pp. 2486–2496, Oct. 2018. DOI: 10.1109/JSAC.2018.2874145.
- [99] A. Perez, A. Fouda, and A. S. Ibrahim, “Ray tracing analysis for UAV-assisted integrated access and backhaul millimeter wave networks,” in *Proc. of the IEEE Internat. Symp. on “A World of Wireless, Mobile and Multimedia Netw.” (WoWMoM)*, Washington DC, USA, Aug. 2019, pp. 1–5. DOI: 10.1109/WoWMoM.2019.8792969.
- [100] E. Kalantari, M. Z. Shakir, H. Yanikomeroglu, and A. Yongacoglu, “Backhaul-aware robust 3D drone placement in 5G+ wireless networks,” in *Proc. of the IEEE Internat. Conf. on Commun. Workshops (ICC Workshops)*, Paris, France, Jul. 2017, pp. 109–114. DOI: 10.1109/ICCW.2017.7962642.
- [101] A. Fouda, A. S. Ibrahim, I. Guvenc, and M. Ghosh, “UAV-based in-band integrated access and backhaul for 5G communications,” in *Proc. of the IEEE Vehic. Tech. Conf. (VTC)*, Chicago, IL, USA, Apr. 2018, pp. 1–5. DOI: 10.1109/VTCFall.2018.8690860.
- [102] A. Fouda, A. S. Ibrahim, I. Guvenc, and M. Ghosh, “Interference management in uav-assisted integrated access and backhaul cellular networks,” *IEEE Access*, vol. 7, pp. 104 553–104 566, Jul. 2019. DOI: 10.1109/ACCESS.2019.2927176.
- [103] C. Qiu, Z. Wei, Z. Feng, and P. Zhang, “Joint resource allocation, placement and user association of multiple uav-mounted base stations with in-band wireless backhaul,” *IEEE Wireless Commun. Lett.*, vol. 8, no. 6, pp. 1575–1578, Dec. 2019. DOI: 10.1109/LWC.2019.2928544.
- [104] E. Kalantari, I. Bor-Yaliniz, A. Yongacoglu, and H. Yanikomeroglu, “User association and bandwidth allocation for terrestrial and aerial base stations with backhaul considerations,” in *Proc. of the IEEE Personal, Indoor and Mob. Radio Commun. (PIMRC)*, Montreal, Canada, Oct. 2017, pp. 1–6. DOI: 10.1109/PIMRC.2017.8292783.
- [105] H. Zhang and L. Dai, “Mobility prediction: A survey on state-of-the-art schemes and future applications,” *IEEE Access*, vol. 7, pp. 802–822, Dec. 2019, ISSN: 2169-3536. DOI: 10.1109/ACCESS.2018.2885821.
- [106] L. Zhang and N. Ansari, “A framework for 5G networks with in-band full-duplex enabled drone-mounted base-stations,” *IEEE Wireless Commun.*, vol. 26, no. 5, pp. 121–127, Feb. 2019. DOI: 10.1109/MWC.2019.1800486.
- [107] L. Zhang and N. Ansari, “Backhaul-aware uplink communications in full-duplex DBS-aided HetNets,” in *Proc. of the IEEE Global Telecommun. Conf. (GLOBECOM)*, Waikoloa, HI, USA, Dec. 2019, pp. 1–6. DOI: 10.1109/GLOBECOM38437.2019.9013471.
- [108] N. Tafintsev, D. Moltchanov, M. Gerasimenko, M. Gapeyenko, J. Zhu, S.-p. Yeh, N. Himayat, S. Andreev, Y. Koucheryavy, and M. Valkama, “Aerial access and backhaul in mmWave B5G systems: Performance dynamics and optimization,” *IEEE Commun. Mag.*, vol. 58, no. 2, pp. 93–99, Feb. 2020. DOI: 10.1109/MCOM.001.1900318.
- [109] A. A. Khuwaja, Y. Zhu, G. Zheng, Y. Chen, and W. Liu, “Performance analysis of hybrid UAV networks for probabilistic content caching,” *IEEE Syst. J.*, pp. 1–12, Aug. 2020. DOI: 10.1109/JSYST.2020.3013786.
- [110] P. Agyapong *et al.*, “Simulation guidelines,” METIS, Deliverable 6.1, Oct. 2013. [Online]. Available: https://metis2020.com/wp-content/uploads/deliverables/METIS_D6.1_v1.pdf (visited on 09/20/2021).
- [111] Y. Sui, I. Guvenc, and T. Svensson, “Interference management for moving networks in ultra-dense urban scenarios,” *Journal of Wireless Commun. and Netw.*, vol. 111, pp. 1–32, Apr. 2015. DOI: 10.1186/s13638-015-0326-1.
- [112] 3GPP, “Study on channel model for frequencies from 0.5 to 100 GHz,” 3rd Generation Partnership Project (3GPP), TR 38.901, Sep. 2017, v.14.2.0. [Online]. Available: <http://www.3gpp.org/DynaReport/38901.htm> (visited on 09/26/2017).
- [113] A. M. Pessoa, I. M. Guerreiro, C. F. M. e Silva, T. F. Maciel, D. A. Sousa, D. C. Moreira, and F. R. P. Cavalcanti, “A stochastic channel model with dual mobility for 5G massive networks,” *IEEE Access*, vol. 7, pp. 149 971–149 987, Oct. 2019, ISSN: 2169-3536. DOI: 10.1109/ACCESS.2019.2947407.
- [114] 3GPP, “Evolved universal terrestrial radio access (E-UTRA); physical channels and modulation,” 3rd Generation Partnership Project (3GPP), TS 36.211, Jun. 2021, v.16.6.0. [Online]. Available: <http://www.3gpp.org/ftp/Specs/html-info/36211.htm>.
- [115] —, “NR; physical layer measurements,” 3rd Generation Partnership Project (3GPP), TS 38.215, version v.15.3.0, Sep. 2018. [Online]. Available: <http://www.3gpp.org/ftp/Specs/html-info/38215.htm> (visited on 10/15/2018).
- [116] —, “NR; physical layer procedures for data,” 3rd Generation Partnership Project (3GPP), TS 38.214, Dec. 2017, v.15.0.0. [Online]. Available: <http://www.3gpp.org/ftp/Specs/html-info/38214.htm>.
- [117] —, “Study on evaluation methodology of new vehicle-to-everything (V2X) use cases for LTE and NR,” 3rd Generation Partnership Project (3GPP), TS 37.885, Dec. 2018, v.15.2.0. [Online]. Available: <http://www.3gpp.org/ftp/Specs/html-info/37885.htm> (visited on 04/17/2019).
- [118] V. F. Monteiro, F. R. M. Lima, D. C. Moreira, D. A. Sousa, T. F. Maciel, B. Makki, R. Shreevastav, and H. Hannu. (Apr. 2022). “TDD frame design for interference handling in mobile IAB networks.” arXiv: 2204.13198 [cs.SY].
- [119] 3GPP, “IAB Enhancements for Rel 17,” 3rd Generation Partnership Project (3GPP), RP 192709, Dec. 2019, TSG-RAN WG3 meeting no. 86. [Online]. Available: https://www.3gpp.org/ftp/TSG_RAN/TSG_RAN/TSGR_86/Docs/RP-192709.zip (visited on 09/13/2021).
- [120] —, “IAB topology update procedure,” 3rd Generation Partnership Project (3GPP), R3 212413, May 2021, TSG-RAN WG3 meeting no. 112-e. [Online]. Available: https://www.3gpp.org/ftp/TSG_RAN/WG3_Iu/TSGR3_112-e/Docs/R3-212413.zip (visited on 09/13/2021).
- [121] —, “Principles of Group Mobility for Inter-donor IAB-node Migration,” 3rd Generation Partnership Project (3GPP), R3 206332, Nov. 2020, TSG-RAN WG3 meeting no. 110-e. [Online]. Available: https://www.3gpp.org/ftp/TSG_RAN/WG3_Iu/TSGR3_110-e/Docs/R3-206332.zip (visited on 09/13/2021).



Victor F. Monteiro received the double B.Sc. degree in General Engineering, from the École Centrale Lyon, France and in Telecommunications Engineering (magna cum laude), from the Federal University of Ceará (UFC), Fortaleza, Brazil, in 2013. In 2015 and 2019, he received the M.Sc. and PhD degrees in Telecommunications Engineering from UFC, respectively. He is currently a Postdoctoral researcher at the Wireless Telecommunications Research Group (GTel), UFC, where he works in projects in cooperation with Ericsson Research. In 2016, he was an invited researcher at Ericsson Research in Lulea, Sweden, where he worked for 6 months on the topic of LTE-NR Dual Connectivity. Besides, in 2017/2018, he spent one year at Ericsson Research in Stockholm, Sweden, where he worked on the topics of mobility management and channel hardening. From 2010 to 2012, he took part, in France, of the Eiffel Excellence Scholarship Program, established by the French Ministry of Foreign Affairs. His research interests include machine learning, 5G architecture and protocols, 5G measurement and reporting procedures, mobility management and radio resource allocation.



Fco. Rafael M. Lima received the B.Sc. degree with honors in Electrical Engineering in 2005, and M.Sc. and D.Sc. degrees in Telecommunications Engineering from the Federal University of Ceará, Fortaleza, Brazil, in 2008 and 2012, respectively. In 2008, he has been in an internship at Ericsson Research in Lulea, Sweden, where he studied scheduling algorithms for LTE system. Since 2010, he has been a Professor of Computer Engineering Department of Federal University of Ceará, Sobral, Brazil. Prof. Lima is also a senior member of IEEE

and senior researcher at the Wireless Telecom Research Group (GTEL), Fortaleza, Brazil, where he works in projects in cooperation with Ericsson Research. He has published several conference and journal articles as well as patents in the wireless telecommunications field. His research interests include radio resource allocation algorithms for QoS guarantees for 5G and beyond 5G networks in scenarios with multiple services, resources, antennas and users.



Darlan C. Moreira received B.Sc. degree in electrical engineering in 2005 from the Federal University of Ceará (UFC), Fortaleza, Brazil, in 2005. In 2007 and 2020 he received the M.S. and Ph.D. degrees, respectively, in Teleinformatics Engineering from the same institution. In 2007, he was an invited researcher at Ericsson Research in Kista, Sweden, where he worked for 3 months. In 2010, he was an invited researcher at Supélec in Gif-sur-Yvette, France, for 6 months. Since 2005 he has been a researcher at Wireless

Telecommunications Research Group (GTEL), Brazil, where he has been working in projects within the technical cooperation between GTEL and Ericsson Research. Some topics of his research interests include machine learning, MIMO transceiver design, channel estimation, interference management, integrated access and backhaul, and modeling and simulation of cellular communication.



Diego A. Sousa received the B.Sc. degree in Computer Engineering in University of Ceará (UFC), Sobral, Brazil, in 2011. He received M.Sc. and Ph.D. degree in Teleinformatics Engineering from the UFC, Fortaleza, Brazil, in 2013 and 2018, respectively. Since 2013, he has been a researcher at the Wireless Telecom Research Group (GTEL), UFC, participating of projects in a technical and scientific cooperation with Ericsson Research. Also, since 2013, he has been a Professor of the Federal Institute of Education, Science, and

Technology of Ceará (IFCE), Paracuru, Brazil. His research interests include numerical optimization, 5G networks, coordinated scheduling, radio resource management for QoS/QoE provisioning.



Tarcisio F. Maciel received his B.Sc. and M.Sc. degrees in Electrical Engineering from the Federal University of Ceará (UFC) in 2002 and 2004, respectively, and his Dr.Ing. degree from Technische Universität Darmstadt (TUD), Germany, in 2008, also in Electrical Engineering. Since 2001, he has actively participated in several projects in a technical and scientific cooperation between the Wireless Telecommunications Research Grupo (GTEL), UFC, and Ericsson Research. From 2005 to 2008, he was a research assistant with the Communications

Engineering Laboratory, TUD. Since 2008, he has been a member of the Post-Graduation Program in Teleinformatics Engineering, UFC. In 2009, he was a Professor of computer engineering with UFC-Sobral and since 2010, he has been a Professor with the Center of Technology, UFC. His research interests include radio resource management, numerical optimization and multi-user/multi-antenna communications.



Behrooz Makki (Senior Member, IEEE) received the Ph.D. degree in communication engineering from Chalmers University of Technology, Gothenburg, Sweden. He was a Postdoctoral Researcher with the Chalmers University of Technology from 2013 to 2017. He is currently working as a Senior Researcher with Ericsson Research, Gothenburg, Sweden. He has co-authored 67 journal papers, 47 conference papers, and 90 patent applications. His current research interests include integrated access and backhaul, green communications, millimeter

wave communications, NOMA, and backhauling. Behrooz is a recipient of the VR Research Link Grant, Sweden, in 2014, the Ericsson's Research Grant, Sweden, in 2013, 2014, and 2015, the ICT SEED Grant, Sweden, in 2017, as well as the Wallenbergs Research Grant, Sweden, in 2018. Also, he is a recipient of the IEEE Best Reviewer Award for IEEE TRANSACTIONS ON WIRELESS COMMUNICATIONS in 2018, and the IEEE Best Editor Award for IEEE WIRELESS COMMUNICATIONS LETTERS in 2020. He is currently working as an Editor for IEEE TRANSACTIONS ON COMMUNICATIONS, IEEE WIRELESS COMMUNICATIONS LETTERS, and IEEE COMMUNICATIONS LETTERS. He was a member of the European Commission projects "mm-Wave Based Mobile Radio Access Network for 5G Integrated Communications" and "ARTIST4" as well as various national and international research collaborations.



Hans Hannu is a Master Research Engineer at Ericsson Research since 2011. He holds a M. Sc. in Electrical Engineering / Signal Processing from Luleå University of Technology, 1998, Sweden. Hans works in areas as service realization and performance over cellular networks, including radio access and network transport protocol, with algorithm development, such as data transmission scheduling, and project management. He has co-authored 47 granted patents.